

# Do co-jumps impact correlations in currency markets?

Jozef Barunik<sup>a,b,\*</sup>, Lukas Vacha<sup>a,b</sup>

<sup>a</sup>*Institute of Economic Studies, Charles University in Prague, Opletalova 26, 110 00 Prague, Czech Republic*

<sup>b</sup>*Institute of Information Theory and Automation, The Czech Academy of Sciences, Pod Vodarenskou Vezi 4, 182 00 Prague, Czech Republic*

---

## Abstract

We study how co-jumps influence covariance and correlation in currency markets. We propose a new wavelet-based estimator of quadratic covariation that is able to disentangle the continuous part of quadratic covariation from co-jumps. The proposed estimator is able to identify the statistically significant co-jumps that impact covariance structures by using bootstrapped test statistics. Empirical findings reveal the behavior of co-jumps during Asian, European and U.S. trading sessions. Our results show that the impact of co-jumps on correlations increased during the years 2012 – 2015. Hence appropriately estimating co-jumps is becoming a crucial step in understanding dependence in currency markets.

*Keywords:* co-jumps, currency markets, realized covariance, wavelets, bootstrap

---

*JEL:* C14, C53, G17

---

<sup>☆</sup>The support from the Czech Science Foundation under the 13-32263S and 13-24313S projects is gratefully acknowledged.

<sup>\*</sup>Corresponding author, Tel. +420(602)161710, Email address: vachal@utia.cas.cz

## 1. Introduction

An accurate framework for covariance estimation is crucial for asset pricing, risk management and portfolio optimization. The recent financial and sovereign debt crisis reminded us once again how global markets are interdependent and increased the demand for an accurate estimation of covariances. Although most studies have focused on the precise estimation of integrated covariance structures, the role of co-jumps in overall correlations remains incompletely understood. In this paper, we focus on estimating significant co-jumps in currency markets and answering the following question: “Do co-jumps impact correlations?”. For this reason, we propose a wavelet-based methodology for estimating co-jumps together with bootstrapped test statistics and adjusted the noise-robust covariance estimator. We argue that co-jumps represent an important part of the (total) quadratic covariation of the currency markets, and our framework for co-jump detection improves estimates of the true covariance process. In addition, we examine the co-jump, covariance, and correlation estimates for the three main trading sessions—Asian, European and the U.S.—to determine where the dependence is being created.

The increasing availability of high-frequency intraday data has allowed a shift from parametric conditional covariance estimation based on daily data toward model-free measurements of so-called “realized quantities” using intraday data. Using a seminal result in semi-martingale process theory, Andersen et al. (2003) show that realized variance becomes a consistent estimator of integrated variance with increasing sampling frequency under the assumption of no jumps and zero microstructure noise. Barndorff-Nielsen and Shephard (2004a) generalize the idea to a multivariate setting of so-called “realized covariation” and provide an asymptotic distribution theory for covariance (and correlation) analysis, again assuming zero microstructure noise and no jumps. Although the theory is appealing and intuitive, it assumes that the observed high-frequency data represent the true underlying process. Nevertheless, the real-world data are contaminated with microstructure noise and jumps, which makes drawing statistical inferences rather difficult. As a result, realized measures suffer from large bias because of the presence of noise and jumps in the observed data.

To address the bias in estimation, researchers often collect sparsely sampled observations. This approach reduces the bias but discards a very large amount of data directly. Although it is statistically implausible, the reason is based on an empirical observation of increasing biases with increasing data-collection frequency. The desire to use all available data at higher frequencies led to the recent publication of a number of proposed approaches to restore the consistency through subsampling, for example, Zhang et al. (2005)’s two-scale realized volatility estimator. Zhang (2011)

generalizes these ideas to a multivariate setting and defines a two-scale covariance estimator. Barndorff-Nielsen et al. (2011) achieve positive semi-definiteness of the variance-covariance matrix using multivariate kernel-based estimation. Furthermore, Griffin and Oomen (2011) and Aït-Sahalia et al. (2010) address microstructure noise and non-synchronous trading and propose a consistent and efficient estimator of realized covariance. Aït-Sahalia and Jacod (2012) analyze the effects of microstructure noise and jumps, and Varneskov (2016) estimate quadratic covariation using a general multivariate additive noise model.

In addition to the microstructure noise, ignoring jumps and co-jumps can substantially influence results of estimation, especially with regard to forecasting, option pricing, portfolio risk management and credit risk management (Jawadi et al., 2015). The empirical interest in jumps and, recently, co-jumps is motivated by the significant consequences of possibly misspecifying price processes. To resolve this problem, Barndorff-Nielsen and Shephard (2006) introduce a test based on the difference between the bipower variation and the quadratic variation. Andersen et al. (2007) and Huang and Tauchen (2005) investigate multipower variations to assess the proportion of the quadratic variation attributable to jumps. In addition, Andersen et al. (2007) and Lee and Mykland (2008) introduce two very similar procedures that compare intraday returns to a local volatility measure. Recently, Novotný et al. (2015) use Lee and Mykland (2008)’s procedure to identify jump clusters on currency markets. Jiang and Oomen (2008) construct a test based on the hedging error of a variance swap replication strategy. Aït-Sahalia and Jacod (2009) propose an estimator of truncated power variations computed at different sampling frequencies. This approach was further extended in Jacod and Todorov (2009). Furthermore, Andersen et al. (2010) develop a sequential jump detection scheme that allows for direct identification of the intraday times and sizes of price jumps. Finally, Andersen et al. (2012) report a test for jumps constructed using the MedRV and MinRV measures. Other tests include those of Mancini (2009) and Lee and Hannig (2010).

Building on univariate jump detection, the literature has recently focused on detecting co-jumps and multi-jumps. Bollerslev et al. (2008) detect co-jumps in a large panel of intraday stock returns in equally weighted portfolio. They propose a mean cross-product statistic that directly measures how closely the stocks co-move. Lahaye et al. (2011) use Lee and Mykland (2008)’s univariate jump test to identify co-jumps, defined as jumps occurring simultaneously on different markets. They call this approach “univariate co-jumps” because their detection relies on univariate jump detection. In addition, Mancini and Gobbi (2012) observe co-jumps via thresholding techniques. Recently, spectral techniques for co-jump detection have been employed by Bibinger and Winkelmann (2015). Gilder et al. (2014) use the

approach of Bollerslev et al. (2008) to identify co-jumps daily. Because this method is not robust against disjoint co-jumps, these authors further utilize tests for intraday jumps, as described by Andersen et al. (2010). A test statistic that can explicitly identify co-jumps is proposed in Gnabo et al. (2014) and accounts for the asset’s covariation, considering a co-jump in terms of large returns’ product with respect to local covariation. A common problem associated with this method is that it can lead to false co-jump detection when a substantially large jump occurs in only one asset. Extension to a multivariate space is proposed by Caporin et al. (2014), who use a formal test to detect multi-jumps in larger portfolios. Their procedure is based on comparing two types of smoothed power variations.

In this work, we contribute to the growing literature by introducing an approach based on a wavelet decomposition of stochastic processes. We apply wavelets to covariance estimation and jump and co-jump detection. Wavelets have been used successfully in the estimation of jumps and volatility (Fan and Wang, 2007; Xue et al., 2014; Barunik and Vacha, 2015), although to the best of our knowledge, we are the first to extend these ideas to estimating covariance and co-jumps. Hence, we build on the current co-jump literature by providing a technique that allows for precise jump and co-jump detection while minimizing false co-jumps resulting from large idiosyncratic jumps. Moreover, we improve the finite sample properties of the jump and co-jump tests based on realized measures by extending the bootstrap tests developed in a univariate setting (Dovonon et al., 2014). The estimator we propose is based on the two-scale covariance estimator framework of Zhang (2011), and thus, it is able to utilize all available data using an unbiased estimator in the presence of noise. We test the small sample performance of the estimator in a large numerical study and compare it to other popular integrated covariation estimators under different simulation settings with varying noise and co-jump levels. The results show that our wavelet-based estimator can estimate the realized covariance and correlation from data containing microstructure noise, jumps, and co-jumps with high precision.

Finally, the estimator is applied to real data, thus allowing us to better understand how co-jumps impact covariance and correlations in currency markets. Empirical findings reveal the behavior of co-jumps during Asian, European and U.S. trading sessions. Our results show that the proportion of co-jumps relative to the covariance increased during the years 2012 – 2015. Hence, the impact of co-jumps on correlations increased, and appropriately estimating co-jumps is becoming a crucial step in understanding dependence in currency markets.

## 2. Estimating integrated covariance matrix and co-jumps

Let  $(\mathbf{Y}_t)_{t \in [0, T]}$  be the  $d$ -variate observed (log) price process with  $\ell = 1, \dots, d$  components  $Y_{t, \ell}$  representing currency prices. The common assumption regarding the observed prices is that we can decompose the prices into an underlying (log) price process  $(\mathbf{X}_t)_{t \in [0, T]}$  and a zero mean i.i.d. noise term  $(\boldsymbol{\epsilon}_t)_{t \in [0, T]}$  with finite variance that captures microstructure noise. Furthermore, we assume the noise to be independent of the price process. Thus, the observed price process used here is of the form  $\mathbf{Y}_t = \mathbf{X}_t + \boldsymbol{\epsilon}_t$ .

Let the  $\ell_1$ -th and  $\ell_2$ -th component of the signal (or latent) process  $\mathbf{X}_t$  evolve over time as

$$dX_{t, \ell_1} = \mu_{t, \ell_1} dt + \sigma_{t, \ell_1} dB_{t, \ell_1} + dJ_{t, \ell_1} \quad (1)$$

$$dX_{t, \ell_2} = \mu_{t, \ell_2} dt + \sigma_{t, \ell_2} dB_{t, \ell_2} + dJ_{t, \ell_2}, \quad (2)$$

for  $\ell_1, \ell_2 \in 1, \dots, d$ , where  $\mu_{t, \ell_i}$  and  $\sigma_{t, \ell_i}$  are càdlàg stochastic processes,  $B_{t, \ell_i}$  is a standard Brownian motion correlated with  $\rho_t^{\ell_1, \ell_2} = \text{corr}(B_{t, \ell_1}, B_{t, \ell_2})$ , and  $J_{t, \ell_i}$  denotes a (right-continuous) pure jump process for  $i = \{1, 2\}$ . We assume the jump process to have a finite activity, i.e., only a finite number of jumps occur in a finite time interval, and the jump processes can be correlated.

Following standard statistical methods (Protter, 1992), the quadratic return co-variation associated with  $(X_{t, \ell_1}, X_{t, \ell_2})$  can be decomposed into two parts: the integrated covariance of the latent price process,  $IC_{\ell_1, \ell_2}$  and the co-jump variation  $CJ_{\ell_1, \ell_2}$ . Then, the quadratic covariation over the fixed time interval  $[0, T]$  is

$$QV_{\ell_1, \ell_2} = \underbrace{\int_0^T \sigma_{t, \ell_1} \sigma_{t, \ell_2} d\langle B_{\ell_1}, B_{\ell_2} \rangle_t}_{IC_{\ell_1, \ell_2}} + \underbrace{\sum_{0 \leq t \leq T} \Delta J_{t, \ell_1} \Delta J_{t, \ell_2}}_{CJ_{\ell_1, \ell_2}}. \quad (3)$$

Note that the term  $\Delta J_{t, \ell_1} \Delta J_{t, \ell_2}$  is non-zero only if a co-jump occurs, i.e., when both  $\Delta J_{t, \ell_1}$  and  $\Delta J_{t, \ell_2}$  are non-zero. We denote the quadratic covariation matrix  $\mathbf{QV}$  holding the quadratic variation for  $\ell_1 = \ell_2$  on the diagonal and that for  $\ell_1 \neq \ell_2$  elsewhere as

$$\mathbf{QV} = \begin{pmatrix} QV_{\ell_1, \ell_1} & QV_{\ell_1, \ell_2} \\ QV_{\ell_2, \ell_1} & QV_{\ell_2, \ell_2} \end{pmatrix}. \quad (4)$$

Using continuous and discontinuous parts, the quadratic covariation matrix is further decomposed as

$$\mathbf{QV} = \mathbf{IC} + \mathbf{CJ} = \begin{pmatrix} IC_{\ell_1, \ell_1} + CJ_{\ell_1, \ell_1} & IC_{\ell_1, \ell_2} + CJ_{\ell_1, \ell_2} \\ IC_{\ell_2, \ell_1} + CJ_{\ell_2, \ell_1} & IC_{\ell_2, \ell_2} + CJ_{\ell_2, \ell_2} \end{pmatrix}. \quad (5)$$

A simple estimator of the quadratic covariation in the price processes is the well-known realized covariance, which was introduced by Andersen et al. (2003) and Barndorff-Nielsen and Shephard (2004a). The realized covariance over a fixed time interval  $[0 \leq t \leq T]$  can be estimated as

$$\widehat{QV}_{\ell_1, \ell_2}^{(RC)} = \sum_{i=1}^N \Delta_i Y_{t, \ell_1} \Delta_i Y_{t, \ell_2}, \quad (6)$$

where  $\Delta_i Y_{t, \ell} = Y_{t+i/N, \ell} - Y_{t+(i-1)/N, \ell}$  is the  $i$ -th intraday return over the fixed time interval  $[0, T]$ .

A limit theorem for stochastic processes states that the realized covariance estimator is a consistent estimator of quadratic covariation  $QV_{\ell_1, \ell_2}$  as the number of intraday observations  $i = 1, \dots, N$ , goes to infinity, provided that the processes are not contaminated with microstructure noise and jumps. The details of this result can be found in Andersen et al. (2003) and Barndorff-Nielsen and Shephard (2004a). Hence,  $\widehat{QV}_{\ell_1, \ell_2}^{(RC)}$  estimates the quadratic covariation associated with  $(Y_{t, \ell_1}, Y_{t, \ell_2})$  rather than  $(X_{t, \ell_1}, X_{t, \ell_2})$ . Several estimators capable of recovering the quadratic covariation of the latent process from observed data has recently been proposed in the literature. A two-scale covariance estimator (Zhang, 2011) based on subsampling and multivariate kernel-based estimation (Barndorff-Nielsen et al., 2011), which provides a positive semi-definite variance-covariance matrix, are the most notable frameworks. These approaches can estimate the quadratic variation associated with  $(X_{t, \ell_1}, X_{t, \ell_2})$  and assume zero jumps in the underlying process. In the next section, we propose an estimator building on the ideas described in the literature that will be able to estimate both parts of the quadratic variation of the true price process based on wavelet analysis.

### 2.1. Wavelet decomposition of quadratic covariation

Our estimators of quadratic covariation, integrated covariation and co-jumps are based on wavelet analysis. Whereas most time series models are naturally set in the time domain, Fan and Wang (2007) and later Barunik and Vacha (2015); Barunik et al. (2016) enrich the estimation of quadratic variation with wavelets and frequency domain. Traders in the currency markets have heterogeneous expectations and operate on different horizons ranging from minutes to days or even months. Thus, the frequency domain can be helpful not only in improving the covariance estimation but also in decomposing the covariance into different investment horizons because wavelets allow for time-scale decomposition of stochastic processes (Antoniu and Gustafson, 1999) and are energy preserving. Importantly, wavelets have been used

successfully to estimate jumps (Fan and Wang, 2007; Xue et al., 2014), volatility, risk (Gençay et al., 2005). Thus, formulating covariance estimators will be a useful generalization.

Let us start with wavelet decomposition of the quadratic variation on the diagonal terms in the covariance matrix  $\mathbf{QV}$ . The quadratic variation over a fixed time interval  $[0 \leq t \leq T]$  associated with  $Y_{t,\ell} \in L^2(\mathbb{R})$  can be written as

$$QV_\ell = \|Y_{t,\ell}\|^2 = \frac{1}{C_\psi} \int_0^\infty \left[ \int_{-\infty}^\infty |W_{j,k}^\ell|^2 dk \right] \frac{dj}{j^2}, \quad (7)$$

where  $W_{j,k}^\ell$  is the continuous wavelet transform with respect to a wavelet  $\psi_{j,k}(t) = |j|^{-1/2} \psi\left(\frac{t-k}{j}\right)$  defined as:

$$W_{j,k}^\ell = |j|^{-1/2} \int_0^T \overline{\psi\left(\frac{t-k}{j}\right)} \Delta Y_{t,\ell} dt, \quad (8)$$

where  $\Delta Y_{t,\ell} = (\Delta_1 Y_{t,\ell}, \dots, \Delta_N Y_{t,\ell})$  are intraday returns,  $k$  is a position,  $j$  is a scale of wavelet  $\psi$ , and the bar denotes complex conjugation<sup>1</sup>. Eq.(7) shows how the quadratic variation of a process  $Y_{t,\ell}$  can be decomposed by the wavelet transform. Furthermore, we can generalize this result to a quadratic covariation. If  $(Y_{t,\ell_1}, Y_{t,\ell_2})$  belong to  $L^2(\mathbb{R})$  and have a continuous wavelet transform, then the quadratic covariation can be decomposed by wavelets in a similar manner as

$$QV_{\ell_1, \ell_2} = \frac{1}{C_\psi} \int_0^\infty \left[ \int_{-\infty}^\infty W_{j,k}^{\ell_1} \overline{W_{j,k}^{\ell_2}} dk \right] \frac{dj}{j^2}. \quad (9)$$

Eq.(9) is a starting point for the construction of a wavelet estimator of quadratic covariation. The term  $\int_{-\infty}^\infty W_{j,k}^{\ell_1} \overline{W_{j,k}^{\ell_2}} dk$  expresses the quadratic covariation at a particular scale  $j$ , whereas the other integral sums all of the available scales  $j$ . Using this representation, we can know the exact contribution of each scale to the overall quadratic covariation measure.

## 2.2. Time-scale decomposition of covariance in discrete time

Since we estimate the quadratic covariation on discrete data, we use a non-subsampled version of a discrete wavelet transform, more specifically, the maximal overlap discrete wavelet transform (MODWT).<sup>2</sup> The idea of the discrete form of the

---

<sup>1</sup>For more details about the continuous wavelet transform, see Daubechies (1992)

<sup>2</sup>A brief introduction of the discrete wavelet transform and MODWT can be found in Appendix A.

estimator is based on the continuous form defined above in the Eq.(9). In contrast to the continuous wavelet transform the discrete version uses scales that are not continuous but represent frequency bands. In our discrete setting, we work with  $i = 1, \dots, N$  intraday observations over  $t = 0, \dots, T$  days.

The integrated covariance of the discrete process  $(Y_{t,\ell_1}, Y_{t,\ell_2})$  that belongs to  $L^2(\mathbb{R})$  over a fixed time horizon  $[0 \leq t \leq T]$  can be expressed as a discrete wavelet decomposition on a scale-by-scale basis. Hence, for a particular scale  $j \in (1, 2, \dots, \mathcal{J}^m)$ , we write:

$$QV_{\ell_1, \ell_2}(j) = \sum_{k=1}^N \mathcal{W}_{j,k}^{\ell_1} \mathcal{W}_{j,k}^{\ell_2}, \quad (10)$$

where  $\mathcal{W}_{j,k}^\ell$  is the intraday MODWT wavelet coefficient, with  $k = 1, \dots, N$  intraday observations, where  $\mathcal{J}^m$  denotes the maximal level of wavelet decomposition. Hence, we use a  $N \times \mathcal{J}^m + 1$  matrix of wavelet coefficients where the first  $\mathcal{J}^m$  subvectors are the MODWT wavelet coefficients at  $j = 1, \dots, \mathcal{J}^m$  levels, and the last subvector consists of the MODWT scaling coefficients at the  $\mathcal{J}^m$  level. We refer to Appendix A for details.

Asymptotically, as the number of intraday elements goes to infinity ( $N \rightarrow \infty$ ), an infinite number of scales can be used. In that case, the covariance between scaling coefficients goes to zero, and the covariance of  $(Y_{t,\ell_1}, Y_{t,\ell_2})$  depends only on the covariance of the wavelet coefficients (for proof, see Appendix B)

$$QV_{\ell_1, \ell_2} = \sum_{j=1}^{\infty} QV_{\ell_1, \ell_2}(j) = \sum_{j=1}^{\infty} \sum_{k=1}^N \mathcal{W}_{j,k}^{\ell_1} \mathcal{W}_{j,k}^{\ell_2}. \quad (11)$$

The application of wavelets in Eq. (11) reveals the contributions of particular wavelet scales (frequency bands) to the overall integrated covariance. Thus, we can identify the parts of the frequency spectrum that are essential for this measure.

### 2.3. Wavelet estimator of quadratic covariation

Using the properties of Eq. (11), we define the wavelet realized covariance estimator  $\widehat{QV}_{\ell_1, \ell_2}^{(WRC)}$  of processes  $(Y_{t,\ell_1}, Y_{t,\ell_2})$  in  $L^2(\mathbb{R})$  over a fixed time horizon  $[0 \leq t \leq T]$  as

$$\widehat{QV}_{\ell_1, \ell_2}^{(WRC)} = \sum_{j=1}^{\mathcal{J}^m+1} \sum_{k=1}^N \mathcal{W}_{j,k}^{\ell_1} \mathcal{W}_{j,k}^{\ell_2}, \quad (12)$$

where  $N$  is the number of intraday observations, and  $\mathcal{J}^m \leq \log_2 N$  is the number of scales considered.  $\mathcal{W}_{j,k}^\ell$  are the MODWT coefficients of the process  $\Delta Y_{t,\ell} =$



$(\Delta_1 Y_{t,\ell}, \dots, \Delta_N Y_{t,\ell})$  on scale  $j$  and are unaffected by the boundary conditions. Using the results of Serroukh and Walden (2000a,b), we can write  $\widehat{QV}_{\ell_1, \ell_2}^{(RC)} = \widehat{QV}_{\ell_1, \ell_2}^{(WRC)}$  because the realized covariance of the zero mean return process over  $[0 \leq t \leq T]$  can be written as

$$\sum_{i=1}^N \Delta_i Y_{t,\ell_1} \Delta_i Y_{t,\ell_2} = \sum_{j=1}^{\mathcal{J}^m+1} \sum_{k=1}^N \mathcal{W}_{j,k}^{\ell_1} \mathcal{W}_{j,k}^{\ell_2}. \quad (13)$$

The estimator in Eq. (12) takes the asymptotic properties of the  $\widehat{QV}_{\ell_1, \ell_2}^{(RC)}$ , and the estimator converges in probability to the quadratic covariation

$$\widehat{QV}_{\ell_1, \ell_2}^{(WRC)} \xrightarrow{p} QV_{\ell_1, \ell_2}. \quad (14)$$

#### 2.4. Co-jump detection

In addition to decomposing covariance into scales, wavelets play important roles in our estimation strategy because we use them to detect co-jumps. In this section, we introduce a wavelet jump detection procedure, which allows us to disentangle the integrated covariance from the co-jump variation. Because the real market data are contaminated with jumps, co-jump detection in the process of generating asset prices is crucial. We assume that the sample path of the price process has a finite number of jumps (a.s.), i.e., we assume finite jump activity. Building on the theoretical results of Wang (1995) regarding wavelet jump detection in deterministic functions with i.i.d. additive noise, which were recently extended to stochastic processes by Fan and Wang (2007), we use the discretized version of the continuous wavelet transform, the MODWT<sup>3</sup>, to localize jumps. Similar to Fan and Wang (2007), we use the first scale of the discrete wavelet transform to distinguish between the continuous and discontinuous parts of the stochastic price process with i.i.d. additive noise. To detect the exact jump location, we use the universal threshold of Donoho and Johnstone (1994) with the intraday median absolute deviation estimator of standard deviation adapted for the MODWT wavelet coefficients (Percival and Walden, 2000). The threshold  $\xi$  has the form:

$$\xi = \frac{\sqrt{2} \text{median}\{|\mathcal{W}_{1,k}^\ell|\}}{0.6745} \sqrt{2 \log N}, \quad (15)$$

where  $\mathcal{W}_{1,k}^\ell$  is a vector of intraday wavelet coefficients. If the absolute value of an intraday wavelet coefficient exceed the threshold  $\xi$ , then the jump will be estimated

---

<sup>3</sup>The advantage of implementing the MODWT is that we are not restricted to a dyadic sample length.

at position  $k$ .<sup>4</sup> In other words, the noise and the continuous part are relatively small, and hence, the dominance of  $\mathcal{W}_{1,k}^\ell$  results from a discontinuous jump. The jump size at intraday position  $i$  is then estimated as

$$\Delta_i J_{t,\ell} = (\Delta_i Y_{t,\ell}) \mathbb{1}_{\{|\mathcal{W}_{1,k}^\ell| > \xi\}}. \quad (16)$$

The jump variation of the  $X_{t,\ell}$  process, denoted as  $CJ_\ell$ , over  $[0 \leq t \leq T]$  in the discrete synchronized time is estimated as the sum of squares of all of the estimated jump sizes as

$$\widehat{CJ}_\ell = \sum_{i=1}^N (\Delta_i J_{t,\ell})^2. \quad (17)$$

Fan and Wang (2007) prove that with Eq. (17), we can estimate the jump variation of the process consistently with the convergence rate  $N^{-1/4}$ , and

$$\widehat{CJ}_\ell \xrightarrow{p} CJ_\ell. \quad (18)$$

Thus, the jump-adjusted price process  $Y_{t,\ell}^{(J)} = Y_{t,\ell} - \widehat{CJ}_\ell$  converges in probability to the continuous part without jumps (Fan and Wang, 2007). Because we focus primarily on the bi-variate setting and estimating the continuous covariance, we must detect co-jumps and estimate the co-jump variation. Let us define the co-jump variation of processes  $(X_{t,\ell_1}, X_{t,\ell_2})$  simply as a sum of co-jumps:

$$\widehat{CJ}_{\ell_1, \ell_2} = \sum_{i=1}^N \Delta_i J_{t,\ell_1} \Delta_i J_{t,\ell_2}. \quad (19)$$

Therefore, a co-jump occurs only if both jumps in process  $(X_{t,\ell_1}, X_{t,\ell_2})$  occur simultaneously. Because jumps can be estimated consistently with wavelets (Barunik and Vacha, 2015; Barunik et al., 2016), we can generalize the concept to the two-dimensional case, and thus, we can estimate co-jump variation consistently.

Finally, because we have estimates of the jump and co-jump variation for process  $(X_{t,\ell_1}, X_{t,\ell_2})$ , the estimated co-jump variation matrix can be written as

$$\widehat{CJ} = \begin{pmatrix} \widehat{CJ}_{\ell_1, \ell_1} & \widehat{CJ}_{\ell_1, \ell_2} \\ \widehat{CJ}_{\ell_2, \ell_1} & \widehat{CJ}_{\ell_2, \ell_2} \end{pmatrix}. \quad (20)$$

---

<sup>4</sup>For the MODWT filters, we must slightly correct the position of the wavelet coefficients to obtain the precise jump position; see Percival and Mofjeld (1997).

The definition of a co-jump can be generalized to a broader class of multivariate processes. Co-jumps are particularly important in portfolio theory. For a large, well-diversified portfolio according to Arbitrage Pricing Theory, idiosyncratic jumps are expected to be diversified away, but common jumps, or co-jumps, remain and may impact the correlations.

## 2.5. Data synchronization: Refresh time

One important theoretical assumption that we did not mention above is that the data are assumed to be synchronized, meaning that the prices of the assets were collected at the same time stamp. In practice, trading is non-synchronous, delivering fresh prices at irregularly spaced times, which differ across stocks. Research focusing on non-synchronous trading has been an active field of financial econometrics in past years; see, for example, Hayashi and Yoshida (2005) and Voev and Lunde (2007). This practical issue induces bias in the estimators and may be partially responsible for the Epps effect (Epps, 1979), a phenomenon of decreasing empirical correlation between the returns of two different stocks with increasing data-sampling frequency.

As noted by Barndorff-Nielsen et al. (2011), stale prices are a key feature of estimating covariances because they induce cross-autocorrelation among asset returns. Thus, the refresh time scheme, which may be used as a measure of staleness,<sup>5</sup> is appropriate for the case of low asset liquidity. Aït-Sahalia et al. (2010) compare various synchronization schemes and find that the estimates do not differ significantly from the estimates obtained using the Refresh Time scheme for the same type of data used here. Thus, we can restrict ourselves to this synchronization scheme. However, we should note that this scheme is not appropriate when the securities are very heterogeneous, especially if one of them is highly illiquid compared to the others.

Let  $N_{t,q}$  be the counting process governing the number of observations in the  $q$ -th asset up to time  $t$ , with times of trades  $t_{1,q}, t_{2,q}, \dots$ . Following Barndorff-Nielsen et al. (2011), we define the refresh time, which we use later in our estimator. We present a generalized multivariate version, but in the subsequent analysis, only the bi-variate setting is used.

The first refresh time for  $t \in [0, 1]$  is defined as

$$\tau_1 = \max(t_{1,1}, \dots, t_{1,q}), \quad (21)$$

for  $q = 1, \dots, d$  assets, and all subsequent refresh times are defined as

$$\tau_{v+1} = \max(t_{1+N_{\tau_v,q},q}, \dots, t_{N_{1+\tau_v,q},q}), \quad (22)$$

---

<sup>5</sup>More precisely, the average time difference between the refresh time and the real time is the measure of staleness.

with the resulting Refresh Time sample being of length  $N$ , whereas  $N_q$  denotes the number of trades for an individual asset  $q$ .  $\tau_1$  is thus the first time that all assets record prices, whereas  $\tau_2$  is the first time that all asset prices are refreshed. In the following analysis, we will set our clock time to  $\tau_v$  when using the estimators. Specifically, we will consider the  $\tau$ -th intraday return of the process  $Y_{t,\ell}$ ,

$$\Delta_\tau Y_{t,\ell} = Y_{t+\tau/N,\ell} - Y_{t+(\tau-1)/N,\ell}.$$

This approach converts the problem into one where the Refreshed Times' sample size  $N$  is determined by the degree of non-synchronicity (Barndorff-Nielsen et al., 2011).

## 2.6. Jump wavelet two-scale covariance (JWTSCV) estimator of integrated covariance

Finally, using the time-synchronized jump-adjusted price process  $(Y_{t,\ell_1}^{(J)}, Y_{t,\ell_2}^{(J)})$ , we can propose an estimator of the integrated covariance,  $IC_{\ell_1,\ell_2}$ , that is robust not only against jumps but also against noise. Further, using wavelet decomposition, we can separate the integrated covariance into  $\mathcal{J}^m + 1$  scale components representing the integrated covariance at various frequency bands. Our estimator uses the two-scale covariance estimator (TSCV) described by Zhang (2011) and wavelet decomposition. More specifically, we decompose the covariance into wavelet scales  $\mathcal{J}^m + 1$ , and on each scale, we estimate the covariance using the TSCV. Finally, we sum all of the wavelet scales to obtain the final estimate of covariance at all frequencies.

Denote  $\widehat{IC}_{\ell_1,\ell_2}^{(JWTSCV)}$  as the jump wavelet TSCV (JWTSCV) estimator of the integrated covariance of the asset return processes  $(X_{t,\ell_1}, X_{t,\ell_2})$  in  $L^2(\mathbb{R})$  over the fixed time interval  $[0 \leq t \leq T]$ . The estimator is defined in terms of the time-synchronized jump-adjusted observed process  $(Y_{t,\ell_1}^{(J)}, Y_{t,\ell_2}^{(J)})$  as

$$\widehat{IC}_{\ell_1,\ell_2}^{(JWTSCV)} = \sum_{j=1}^{\mathcal{J}^m+1} c_N \left( \widehat{IC}_{\ell_1,\ell_2}^{(G,J)}(j) - \frac{\bar{n}_G}{n_S} \widehat{IC}_{\ell_1,\ell_2}^{(WRC,J)}(j) \right). \quad (23)$$

The JWTSCV estimator consists of two parts: The first part is the averaged version of the estimator (12) on a grid size of  $\bar{n} = N/G$  for a specific wavelet scale  $j$ :

$$\widehat{IC}_{\ell_1,\ell_2}^{(G,J)}(j) = \frac{1}{G} \sum_{g=1}^G \sum_{k=1}^N \mathcal{W}_{j,k}^{\ell_1} \mathcal{W}_{j,k}^{\ell_2}, \quad (24)$$

where the MODWT wavelet coefficients  $\mathcal{W}_{j,k}^\ell$  are estimated based on the jump-adjusted process  $\Delta Y_{t,\ell}^{(J)} = (\Delta_1 Y_{t,\ell}^{(J)}, \dots, \Delta_N Y_{t,\ell}^{(J)})$ . The second term in the estimator

(23) denotes the part of the estimator (12) corresponding to a wavelet scale  $j$ :

$$\widehat{IC}_{\ell_1, \ell_2}^{(WRC, J)}(j) = \sum_{k=1}^N \mathcal{W}_{j,k}^{\ell_1} \mathcal{W}_{j,k}^{\ell_2}. \quad (25)$$

The constant  $c_N$  can be tuned for small sample performance,  $\bar{n}_G = (N - G + 1)/G$ , and the same applies for  $\bar{n}_S$  (we use  $S = 1$ , and thus,  $\bar{n}_S = N$ ). Because both  $\widehat{IC}_{\ell_1, \ell_2}^{(G, J)}(j)$  and  $\widehat{IC}_{\ell_1, \ell_2}^{(WRC, J)}(j)$  represent the contributions of a specific wavelet scale  $j$  only, the final estimator  $\widehat{IC}_{\ell_1, \ell_2}^{(JWTSCV)}$  is the sum across all available wavelet scales  $j = 1, \dots, \mathcal{J}^m + 1$ .

Note that the estimator (23) is a sum of the TSCV estimators (Zhang, 2011) for all available wavelet scales, and hence, the overall speed of convergence of the JWTSCV is governed by the TSCV estimator. Because the TSCV estimator has a rather slow rate of convergence of  $N^{-1/6}$  and because the wavelet (variance) covariance estimator converges at rate  $N^{-1/2}$  (Serroukh and Walden, 2000a), the JWTSCV estimator converges at rate of  $N^{-1/6}$ , and the asymptotic variance is not increased by wavelet decomposition as a result of the energy-preserving property of the wavelets. Finally, we can write the following:

$$\widehat{IC}_{\ell_1, \ell_2}^{(JWTSCV)} \xrightarrow{p} IC_{\ell_1, \ell_2}. \quad (26)$$

Estimator (23) converges in probability to the *true* integrated covariance, which is the focus of this analysis. Thus, we define a wavelet-based covariation estimator that is able to estimate the realized covariation consistently in the presence of noise and co-jumps.

Finally, to estimate the full (variance) covariance matrix  $\widehat{IC}^{(JWTSCV)}$ , we must also estimate the diagonal terms: the integrated variances  $\widehat{IC}_{\ell_1, \ell_1}^{(JWTSCV)}$  and  $\widehat{IC}_{\ell_2, \ell_2}^{(JWTSCV)}$ . These diagonal terms are estimated with the JWTSCV estimator on  $Y_{t, \ell_1}^{(J)}$  or  $Y_{t, \ell_2}^{(J)}$  separately. This estimation procedure is similar to the jump wavelet two-scale realized variance (JWTSRV) estimator for integrated variance proposed by Barunik and Vacha (2015). The integrated covariance matrix is

$$\widehat{IC}^{(JWTSCV)} = \begin{pmatrix} \widehat{IC}_{\ell_1, \ell_1}^{(JWTSCV)} & \widehat{IC}_{\ell_1, \ell_2}^{(JWTSCV)} \\ \widehat{IC}_{\ell_2, \ell_1}^{(JWTSCV)} & \widehat{IC}_{\ell_2, \ell_2}^{(JWTSCV)} \end{pmatrix}. \quad (27)$$

With the estimates of the covariance matrix, it is straightforward to compute the correlations from its elements.

### 3. Numerical study of the small sample performance of the JWTSCV estimator

In this section, we investigate the small sample performance of the JWTSCV estimator to determine how well it can recover the true integrated covariation when jumps and noise are present in the observed process. Small sample studies are important for these types of estimators because we are always left with a data sample of finite length. In the simulation, we follow the setup of Barndorff-Nielsen et al. (2011) and simulate a bivariate factor stochastic volatility model for  $X_{t,i}$ ,  $i = \{1, 2\}$  and  $t \in [0, 1]$ . Moreover, we consider jumps in the process as

$$\begin{aligned} dX_{t,i} &= \mu_i dt + \gamma_i \sigma_{t,i} dB_{t,i} + \sqrt{1 - \gamma_i^2} \sigma_{t,i} dW_t + c_{t,i} dN_{t,i} \\ d\sigma_{t,i} &= \exp(\beta_0 + \beta_1 v_{t,i}) \\ dv_{t,i} &= \alpha v_{t,i} dt + dB_{t,i}, \end{aligned} \tag{28}$$

where the elements of  $B_{t,i}$  are independent standard Brownian motions and are independent of  $W_t$ , and  $c_{t,i} dN_{t,i}$  are independent compound Poisson processes with random jump sizes distributed as  $N \sim (0, \sigma_{1,J})$ . We simulate the processes using the Euler scheme at a time interval of  $\delta = 1s$ , each with  $6.5 \times 60 \times 60$  steps  $n = 23,400$ , corresponding to a 6.5-trading hour day. The parameters are set to  $(\mu_1, \mu_2, \beta_0, \beta_1, \alpha, \gamma_1, \gamma_2) = (0, 0, -5/16, 1/8, -1/40, -0.3, -0.3)$ . Each day is restarted with the initial value of  $v_{t,i}$  drawn from a normal distribution  $N(0, (-2\alpha)^{-1})$ . On each simulated path, we estimate  $\hat{\Sigma}_t$  over  $T = 1$  day. The results are computed for samplings of 1 minute, 5 minutes, 30 minutes and 1 hour for the realized covariance in Eq.(6). Moreover, we use the following benchmark estimators: the bipower realized covariance of Barndorff-Nielsen and Shephard (2004b), the two-scale realized covariance of Zhang (2011), the multivariate realized kernel of Barndorff-Nielsen et al. (2011), and our jump wavelet two-scale realized covariance estimator defined by (23). For convenience, when describing the results, we refer to the estimators as RC, BC, TSCV, MRK and JWTSCV, respectively.

We repeat the simulations with different levels of noise and different numbers of jumps, assuming the market microstructure noise,  $\epsilon_t$ , to be normally distributed with different standard deviations:  $(E[\epsilon^2])^{1/2} = \{0, 0.0015\}$ . Thus, we consider simulations with zero noise and 0.15% of the value of the asset price level noise. We also add different levels of jumps, controlled by intensity  $\lambda$  from the Poisson process  $c_{t,i} dN_{t,i}$ , starting with  $\lambda = 0$ , and continue adding jumps with sizes corresponding to a one standard deviation jump change. Moreover, co-jumps and individual jumps are separated as they have very different impacts on the covariance and correlation

measures. We start by simulating prices with only a single co-jump, and then add one jump to each of the bivariate series that are independent of each other because these two types have different impacts on the covariation and correlation. Individual jumps cause positive bias in the realized covariance measures, and if the estimator cannot handle this effect, the correlation will suffer from large negative bias because the denominator of the fraction will be larger. In contrast, co-jumps will logically cause positive bias in the correlation because the numerator, the covariance, will be positively biased. Finally, we compare the bias of all of the estimators for covariance and correlation.

The true spot correlation between  $X_{t,1}$  and  $X_{t,2}$  without noise and jumps is used for as a reference:  $\sqrt{(1 - \gamma_1^2)(1 - \gamma_2^2)}$ , which is equal to 0.91 here. The full spot covariance matrix  $\Sigma_t = \begin{pmatrix} \Sigma_t^{11} & \Sigma_t^{12} \\ \Sigma_t^{12} & \Sigma_t^{22} \end{pmatrix} = \begin{pmatrix} \sigma_{t,1}^2 & \sigma_{t,1,2} \\ \sigma_{t,1,2} & \sigma_{t,2}^2 \end{pmatrix}$ , where  $\sigma_{t,1,2} = \sigma_{t,1}\sigma_{t,2}\rho_t$ , is used to compute the correlation bias in the simulations. We also report the covariation bias,  $\Sigma_t^{12}$ .

The covariation results are reported in Table C.1. Clearly, JWTSCV can efficiently recover the true integrated covariance of the process in the presence of jumps and noise. The bipower realized covariance measure (BC) can handle jumps to some extent, whereas as expected, the two-scale realized covariance (TSCV) consistently estimates the quadratic covariation but not the integrated covariance in the presence of co-jumps. This is the case for the multivariate realized kernels (MRK) as well.

It is interesting to note that the realized covariance is significantly affected by co-jumps in processes, as expected, whereas individual jumps do not have such an effect. Our JWTSCV estimator may thus be important for portfolio management because it can consistently estimate the true covariation of processes that are not influenced by jumps and co-jumps. In the application section, we use this approach and observe how it can improve the results on real data. Interestingly, the sampling frequencies do not reveal any patterns, probably because of the effect of quite large jumps in the simulations. In the case without jumps and noise, we can see that the covariance measures becomes increasingly biased as the sampling frequency increases.

The biases of all of the estimators when calculating the correlation are reported in Table C.2. The results confirm our expectations. The RC is hugely biased when a single large jump occurs in the series, and the correlation is estimated to be 0.4 instead of 0.91. In contrast, co-jumps cause slight positive bias in the correlation measure. The TSCV and MRK estimators generate similar results. The BC reduces the bias significantly and exhibits good finite sample performance for both individual jumps and co-jumps. Our JWTSCV estimator provides significantly lower bias compared to the BC estimator. Indeed, the results show that this estimator has the

lowest bias and standard error by far and, hence, can recover the true correlation unaffected by the presence of jumps and co-jumps in the process.

#### 4. Bootstrapping the co-jumps

The first step in estimating the integrated covariance from the observed data using the JWTSCV estimator is the estimation of jumps and co-jumps. Relying on the effective jump detection of Fan and Wang (2007), the distribution of the estimated jump and co-jump variation is unknown, and thus, a testing strategy using bootstrapping is appropriate. In addition, bootstrapping can significantly improve the finite sample properties of the jump (Dovonon et al., 2014) and co-jump tests based on realized measures. The newly proposed JWTSCV estimator can recover the integrated covariance from processes contaminated with noise and jumps consistently. If we were interested in actually estimating the co-jumps from the observed data, we could compare it to the quadratic covariation estimate, and considering the estimation error of both estimators, a standard Hausman-type test statistic could be proposed. In the univariate setting, Barunik et al. (2016) bootstrap this type of statistic for jump detection. Here, we extend the univariate approach and propose a bootstrap testing procedure to test for the presence of jumps and co-jumps in a given time interval.

Under the null hypothesis of no jumps and co-jumps in the  $(Y_{t,\ell_1}, Y_{t,\ell_2})$  process,

$$\mathcal{H}^0 : \widehat{QV}_{\ell_1, \ell_2}^{(RC)} - \widehat{IC}_{\ell_1, \ell_2}^{(JWTSCV)} = 0 \quad (29)$$

$$\mathcal{H}^A : \widehat{QV}_{\ell_1, \ell_2}^{(RC)} - \widehat{IC}_{\ell_1, \ell_2}^{(JWTSCV)} \neq 0. \quad (30)$$

We propose a simple test statistic that can be used to detect co-jump variation. If a significant difference exists between the quadratic covariation and integrated covariance, then it is highly probable that we will observe a co-jump variation, possibly because of co-jump(s) or large disjoint jump(s). In this case, the  $\mathcal{H}^0$  is rejected for its alternative.

When the null hypotheses of no jumps holds,  $\widehat{QV}_{\ell_1, \ell_2}^{(RC)} - \widehat{IC}_{\ell_1, \ell_2}^{(JWTSCV)}$  is asymptotically independent from  $\widehat{QV}_{\ell_1, \ell_2}^{(RC)}$  conditional on the volatility path, and we can use two independent random variables to set the Hausman-type statistics to test for the presence of jumps. We proceed by scaling  $\widehat{QV}_{\ell_1, \ell_2}^{(RC)} - \widehat{IC}_{\ell_1, \ell_2}^{(JWTSCV)}$  by the difference in the variances of both estimators, which we obtain using a bootstrap procedure.

Under the null hypothesis of no jumps and co-jumps, we generate  $i$  intraday returns  $(r_{i,\ell_1}^*, r_{i,\ell_2}^*)$  with integrated covariance determined based on empirical estimates



as

$$r_{i,\ell_1}^* = \sqrt{\frac{1}{N} \widehat{IC}_{\ell_1,\ell_1}^{(JWTSCV)}} \eta_{i,\ell_1} \quad (31)$$

$$r_{i,\ell_2}^* = \sqrt{\frac{1}{N} \widehat{IC}_{\ell_2,\ell_2}^{(JWTSCV)}} \left( \widehat{\rho}_{\ell_1,\ell_2} \eta_{i,\ell_1} + \sqrt{1 - \widehat{\rho}_{\ell_1,\ell_2}^2} \eta_{i,\ell_2} \right), \quad (32)$$

$$(33)$$

with  $\widehat{\rho}_{\ell_1,\ell_2}$  being the correlation obtained from the  $\widehat{IC}^{(JWTSCV)}$  matrix, and  $\eta_{i,\ell_1} \sim \mathcal{N}(0,1)$  and  $\eta_{i,\ell_2} \sim \mathcal{N}(0,1)$ . Now, we use  $(r_{i,\ell_1}^*, r_{i,\ell_2}^*)$  to compute  $\widehat{QV}_{\ell_1,\ell_2}^{(RC)*}$  and  $\widehat{IC}_{\ell_1,\ell_2}^{(JWTSCV)*}$ . Generating  $b = 1, \dots, B$  realizations, we obtain  $\mathcal{Z}^* = (\mathcal{Z}^{(1)}, \mathcal{Z}^{(2)}, \dots, \mathcal{Z}^{(B)})$  as

$$\mathcal{Z}^* = \frac{\widehat{QV}_{\ell_1,\ell_2}^{(RC)*} - \widehat{IC}_{\ell_1,\ell_2}^{(JWTSCV)*}}{\widehat{QV}_{\ell_1,\ell_2}^{(RC)*}}. \quad (34)$$

which can be used to construct a bootstrap statistic to test the null hypothesis of no co-jumps as

$$\mathcal{Z} = \frac{\frac{\widehat{QV}_{\ell_1,\ell_2}^{(RC)} - \widehat{IC}_{\ell_1,\ell_2}^{(JWTSCV)}}{\widehat{QV}_{\ell_1,\ell_2}^{(RC)}} - E(\mathcal{Z}^*)}{\sqrt{Var(\mathcal{Z}^*)}} \sim \mathcal{N}(0,1). \quad (35)$$

The bootstrap expectation and variance depend on the data. We rely on the assumptions of Donovan et al. (2014). Thus, by identifying days when the co-jump component is present, we can estimate the off-diagonal elements of the covariance matrix  $\widehat{IC}^{(CJWTSCV)}$  as

$$\widehat{IC}_{\ell_1,\ell_2}^{(CJWTSCV)} = \widehat{QV}_{\ell_1,\ell_2}^{(RC)} \mathbb{1}_{\{|\mathcal{Z}| \leq \phi_{1-\alpha/2}\}} + \widehat{IC}_{\ell_1,\ell_2}^{(JWTSCV)} \mathbb{1}_{\{|\mathcal{Z}| > \phi_{1-\alpha/2}\}}, \quad (36)$$

where  $\phi_{1-\alpha/2}$  is a critical value for the two-sided test with a significance level  $\alpha$ . Finally, we estimate all elements of the (continuous) covariance matrix:

$$\widehat{IC}^{(CJWTSCV)} = \begin{pmatrix} \widehat{IC}_{\ell_1,\ell_1}^{(CJWTSCV)} & \widehat{IC}_{\ell_1,\ell_2}^{(CJWTSCV)} \\ \widehat{IC}_{\ell_2,\ell_1}^{(CJWTSCV)} & \widehat{IC}_{\ell_2,\ell_2}^{(CJWTSCV)} \end{pmatrix}. \quad (37)$$

#### 4.1. Exact co-jump detection

Now, we know which days have significant co-jump components. The next step is to determine whether the reason why the null hypothesis of no co-jumps was rejected is because of the presence of co-jump(s) or, alternatively, because of the

occurrence of large idiosyncratic (disjoint) jump(s). Gnabo et al. (2014) show that large idiosyncratic jumps may inflate the test statistic, and thus, co-jumps may be falsely detected. Therefore, there are basically two possible reasons why the null hypothesis was rejected:

1. Co-jumps:  $t \in [0, T]$ :  $\Delta_i J_{t,\ell_1} \Delta_i J_{t,\ell_2} \neq 0$ , i.e., the process is not exactly zero.
2. Disjoint jumps:  $t \in [0, T]$ : the processes  $\Delta_i J_{t,\ell_1}$  and  $\Delta_i J_{t,\ell_2}$  are not both zero (at least one of them), but  $\Delta_i J_{t,\ell_1} \Delta_i J_{t,\ell_2} = 0$

An advantage of our approach is that the exact jump position is obtained by the wavelet analysis; hence, we can successfully eliminate the false co-jump situation caused by high idiosyncratic jump(s). Furthermore, because we know the directions of the jumps, we can distinguish between co-jumps that occur with jumps of the same or different direction on day  $t$ .

## 5. Impact of co-jumps on correlations in currency markets

The main aim of this work is to shed light on the sources of dependence in currency markets, especially relating to the role of co-jumps. The proposed methodology is an efficient way of estimating integrated covariance and correlation, and thus, we use it to determine the relationship between currency pairs. In addition, we study the roles of the different trading sessions during the day. Finally, we are also interested in how co-jumps influence the correlation between currency pairs.

### 5.1. Data description

We study the relationship among the British pound (GBP), Swiss franc (CHF) and euro (EUR) futures, specifically the GBP–CHF, GBP–EUR and CHF–EUR currency pairs. Currency future contracts are traded on the Chicago Mercantile Exchange (CME) on a 24-hour basis and are quoted in the unit value of the foreign currency in US dollars, which makes them comparable. It is advantageous to use currency futures data for this analysis instead of spot currency prices because they embed interest rate differentials and do not suffer from additional microstructure noise from over-the-counter trading. The cleaned data are available from Tick Data, Inc.<sup>6</sup>

It is important to understand the trading system before we proceed with the estimation. In August 2003, CME launched the Globex trading platform, which substantially increased the liquidity of currency futures. On Monday, December 18,

---

<sup>6</sup><http://www.tickdata.com/>

2006, the CME Globex<sup>®</sup> electronic platform started offering nearly continuous 23-hour-a-day trading. The weekly trading cycle begins at 17:00 Central Standard Time (CST) on Sunday and ends at 16:00 CST on Friday. Each day, the trading is interrupted for one hour from 16:00 CST until 17:00 CST. These changes in the trading system dramatically affected trading activity. For this reason, we restrict ourselves to a sample period extending from January 5, 2007 through July 3, 2015, which includes the recent financial crisis. The futures contracts we use are automatically rolled over to provide continuous price records, and thus, we do not have to address different maturities.

The tick-by-tick transactions are recorded in Chicago Time, referred to as Central Standard Time (CST). Therefore, in a given day, trading activity starts at 5:00 pm CST in Asia, continues in Europe and North America, and finally closes at 4:00 pm in Australia. We exclude potential jumps resulting from the one-hour gap in trading from our analysis by redefining the day in accordance with the electronic trading system. Moreover, we eliminate Saturdays and Sundays, US federal holidays, December 24 to December 26, and December 31 to January 2, because of the very low activity on these days, which would bias the estimates.

To analyze the dependence between the currencies, it is crucial that they are synchronized in time. As discussed in Section 2.5, we use the refresh time scheme to synchronize the data. Looking more closely at the higher frequencies, we find that many transactions have a common time stamp. For these occasions, we use arithmetic average values for all observations with the same time stamp. Finally, we redefine the clock according to the refresh time scheme to obtain synchronized data. We use the refresh time scheme for each pair separately to retain as much data as possible in the analysis.

## 5.2. Activity across trading hours

We begin to study the three currency futures by observing trading activities in the different sessions during the day. The trading activity is measured according to volume using 1-minute intervals. For a given minute, we compute the average over the whole sample and thus obtain a clear picture of how trading activity on FX markets is distributed. The 23-hour trading day is divided into three trading sessions: Asia (17:00 – 2:00 CST), which lasts for 9 hours; Europe (2:00 – 8:00 CST), which lasts for 6 hours; and the U.S. (8:00 – 16:00 CST), which lasts for 8 hours. Figure C.1 shows the relatively low volumes in Asia relative to the Europe and the U.S. sessions. Trading activity peaks before the most active U.S. session starts. When we examine the trading activity in terms of currencies, CHF displays the lowest volume, followed by GBP, whereas the most actively traded currency in our selection is EUR.

### 5.3. Covariance and correlation

We measure the true (integrated) covariance of the three currency pairs GBP–CHF, GBP–EUR and CHF–EUR using the newly proposed JWTSCV estimator. The middle rows of Figures C.2–C.4 show the JWTSCV estimates for different trading sessions. Table C.5 summarizes the results. The highest covariance is measured for the CHF–EUR pair, whereas the GBP–CHF pair shows the lowest values. Analogously, for the trading volume, we observe the lowest covariance in the Asian trading sessions and the highest in the U.S. session. The evolution of the covariance over time reveals that all pairs were exposed to increased covariance during the financial crisis of 2007–08 (highlighted in gray in Figures C.2–C.4). Furthermore, increased activity for the CHF–EUR pair can be observed around 2015, which may be partially caused by the strong appreciation of the CHF after the surprising decision of the Swiss national bank to remove its cap on the CHF on January 15, 2015.<sup>7</sup>

Having estimated a covariance matrix, the correlation can be simply recovered from its elements. When examining the correlations of the currency pairs across the trading sessions, we observe generally lower correlations in the Asian session and generally higher correlations in the U.S. session. Additionally, the CHF–EUR exhibits the highest correlation, whereas GBP–CHF has the lowest one. This difference is quite substantial, exceeding 0.25.

The dynamics of the CHF–EUR pair are rich, including two clear periods of very low correlations (mid-2011 and the beginning of 2015), nearing zero. The second period also includes an increased number of co-jumps because of the recent turbulent period of the CHF.

### 5.4. Impact of co-jumps

An important question we would like to address relates to the importance of co-jumps for the currency pairs and how they influence the covariance and correlation estimates. As a first step, we examine the evolution of co-jumps, and then, we analyze the effects co-jumps on correlation and covariance.

Let us start with days where co-jumps play an important role. Figures C.2–C.4 reveal that the number of days with co-jumps is very low in Asia relative to the EU and U.S. trading hours. In addition, Table C.5 shows that less than 10% of the days with co-jumps occur during the Asian session. This may be attributed to the relatively low trading volumes of the currency pairs in Asia and the minimal important news reported when the Asian markets are open. In contrast, the EU and the U.S. sessions exhibit similar proportions of days with co-jumps, indicating

---

<sup>7</sup>The CHF soared more than 30% percent relative to the Euro on January 15, 2015.

that news influencing the currency pairs is nearly equally distributed across these markets.

The magnitude of co-jump variation generally differs across trading sessions. The U.S. session exhibits the highest co-jump variation (Figures C.2-C.4), and we observe the highest number of co-jumps on the days where co-jumps were detected (see Figure C.5), except one hour before the U.S. trading session starts (7:00–8:00 CST), when the highest number of co-jumps is identified. Hence, we conclude that the number of co-jump is maximized during the U.S. session, when low rates of news influencing European currencies are expected. We attribute this finding to the occurrence of the highest contract trading activity.

The news influencing the US session perceives the European currency markets as a one market, and thus, the differences between GBP, CHF and EUR are small from the U.S. perspective. Another important factor that influence the U.S. session is arbitrage. Because all of the currencies are denominated in the U.S. Dollar, large shifts in the USD cause subsequent co-jumps for all other currencies.

The situation is very different in the Asian session, where we observe the lowest number of co-jumps for all three currency pairs (see Figure C.5). This low co-jump variation corresponds to the low covariance, with only approximately 20% of the total covariation contributed by the Asian session.

Co-jumps exhibit interesting dynamics over time, especially in comparison with the covariance. Particularly for the CHF–EUR pair (see Figure C.6), we observe an increasing number of co-jumps in 2013 with a maximum in 2014, despite the maximum values of the covariance being reached near the financial crisis (Figures C.2-C.4).

Because co-jumps are composed of two univariate jumps, it is interesting to investigate whether these jumps have similar (positive co-jumps) or different (negative co-jumps) directions. Closer analysis shows that most co-jumps are positive (see Table C.4), and thus, most of the time, the currency pairs are influenced together in the same direction. The lowest percentage of negative co-jumps occurs in the U.S. session, which is a consequence of our choice of European currency pairs.<sup>8</sup> As such, it is highly unlikely that traders in the US session will differentiate strongly between European currencies, resulting in jumps in the opposite direction and, hence, negative co-jumps. In contrast, during the European trading hours, the currencies are more likely to jump in opposite directions. Consequently, the highest number of negative co-jumps is detected during the European session.

---

<sup>8</sup>Large movements of the USD may also play a role.

### 5.5. Co-jump dynamics over time

The analyses described above indicate that the share of co-jump variation differs across trading hours. Another relevant question is whether the proportion of co-jumps is stable over time. To observe these dynamics, we divide the sample into years and compute the shares of co-jumps in the total covariation corresponding to a given year (see Table Appendix C). The results indicate that co-jump variation increased substantially in 2013 and 2014 for all pairs and all sessions. For example, the CHF–EUR pair during the EU session exhibited the highest share of co-jumps in the whole examined period (Table C.5), more specifically, in 2014, this share accounts for 12%, a significant proportion.

Generally, the occurrence of co-jumps may significantly increase the total covariation. Thus, when we do not estimate co-jump variation appropriately, the correlation may be significantly biased because of the co-jumps. We demonstrate that the accurate detection of jumps and co-jumps is essential to improve the estimation of the correlation, especially very recently.

## 6. Conclusion

In this paper, we investigate how co-jumps impact covariance structures in the currency market. For this purpose, we propose a new jump wavelet two-scale realized covariance estimator and bootstrap testing procedure to identify co-jumps. This newly proposed methodology builds on the current co-jump literature by allowing for precise jump and co-jump detection while minimizing the identification of false co-jumps resulting from the occurrence of large idiosyncratic jumps.

As an empirical application of the proposed methodology, we study the behavior of co-jumps during Asian, European and U.S. trading sessions. Our results show that the proportion of co-jumps relative to the covariance increased during 2012 – 2015. Hence, the impact of co-jumps on correlations increased, and appropriately estimating co-jumps is becoming a crucial step in understanding dependence in currency markets.

## References

- Aït-Sahalia, Y., J. Fan, and D. Xiu (2010). High frequency covariance estimates with noisy and asynchronous financial data. *Journal of the American Statistical Association* 105(492), 1504–1517.
- Aït-Sahalia, Y. and J. Jacod (2009). Testing for jumps in a discretely observed process. *The Annals of Statistics* 37(1), 184–222.

- Aït-Sahalia, Y. and J. Jacod (2012). Analyzing the spectrum of asset returns: Jump and volatility components in high frequency data. *Journal of Economic Literature* 50(4), 1007–1050.
- Andersen, T., T. Bollerslev, F. Diebold, and P. Labys (2003). Modeling and forecasting realized volatility. *Econometrica* 71(2), 579–625.
- Andersen, T. G., T. Bollerslev, and F. X. Diebold (2007). Roughing it up: Including jump components in the measurement, modeling, and forecasting of return volatility. *Review of Economics and Statistics* 89(4), 701–720.
- Andersen, T. G., T. Bollerslev, and D. Dobrev (2007). No-arbitrage semi-martingale restrictions for continuous-time volatility models subject to leverage effects, jumps and i.i.d. noise: Theory and testable distributional implications. *Journal of Econometrics* 138(1), 125–180.
- Andersen, T. G., T. Bollerslev, P. Frederiksen, and M. Ørregaard Nielsen (2010). Continuous-time models, realized volatilities, and testable distributional implications for daily stock returns. *Journal of Applied Econometrics* 25(2), 233–261.
- Andersen, T. G., D. Dobrev, and E. Schaumburg (2012). Jump-robust volatility estimation using nearest neighbor truncation. *Journal of Econometrics* 169(1), 75–93.
- Antoniou, I. and K. Gustafson (1999). Wavelets and stochastic processes. *Mathematics and Computers in Simulation* 49(1-2), 81–104.
- Barndorff-Nielsen, O., P. Hansen, A. Lunde, and N. Shephard (2011). Multivariate realised kernels: Consistent positive semi-definite estimators of the covariation of equity prices with noise and non-synchronous trading. *Journal of Econometrics* 162(2), 149–169.
- Barndorff-Nielsen, O. and N. Shephard (2004a). Econometric analysis of realized covariation: High frequency based covariance, regression, and correlation in financial economics. *Econometrica* 72(3), 885–925.
- Barndorff-Nielsen, O. and N. Shephard (2004b). Power and bipower variation with stochastic volatility and jumps. *Journal of Financial Econometrics* 2(1), 1–48.
- Barndorff-Nielsen, O. and N. Shephard (2006). Econometrics of testing for jumps in financial economics using bipower variation. *Journal of Financial Econometrics* 4(1), 1–30.

- Barunik, J., T. Krehlik, and L. Vacha (2016). Modeling and forecasting exchange rate volatility in time-frequency domain. *European Journal of Operational Research* 251(1), 329–340.
- Barunik, J. and L. Vacha (2015). Realized wavelet-based estimation of integrated variance and jumps in the presence of noise. *Quantitative Finance* 15(8), 1347–1364.
- Bibinger, M. and L. Winkelmann (2015). Econometrics of co-jumps in high-frequency data with noise. *Journal of Econometrics* 184(2), 361–378.
- Bollerslev, T., T. H. Law, and G. Tauchen (2008). Risk, jumps, and diversification. *Journal of Econometrics* 144(1), 234–256.
- Caporin, M., A. Kolokolov, and R. Renò (2014). Multi-jumps. *Available at SSRN 2488603*.
- Daubechies, I. (1992). *Ten lectures on wavelets*. SIAM.
- Donoho, D. L. and I. M. Johnstone (1994). Ideal spatial adaptation by wavelet shrinkage. *Biometrika* 81(3), 425–455.
- Dovonon, P., S. Gonçalves, U. Hounyo, and N. Meddahi (2014). Bootstrapping high-frequency jump tests. Discussion paper, Toulouse School of Economics.
- Epps, T. W. (1979). Comovements in stock prices in the very short run. *Journal of the American Statistical Association* 74(366a), 291–298.
- Fan, J. and Y. Wang (2007). Multi-scale jump and volatility analysis for high-frequency financial data. *Journal of the American Statistical Association* 102(480), 1349–1362.
- Gençay, R., F. Selçuk, and B. Whitcher (2002). *An Introduction to Wavelets and Other Filtering Methods in Finance and Economics*. Academic Press.
- Gençay, R., F. Selçuk, and B. Whitcher (2005). Multiscale systematic risk. *Journal of International Money and Finance* 24(1), 55–70.
- Gilder, D., M. B. Shackleton, and S. J. Taylor (2014). Cojumps in stock prices: Empirical evidence. *Journal of Banking & Finance* 40, 443–459.



- Gnabo, J.-Y., L. Hvozdyk, and J. Lahaye (2014). System-wide tail comovements: A bootstrap test for cojump identification on the S&P 500, US bonds and currencies. *Journal of International Money and Finance* 48, 147–174.
- Griffin, J. and R. Oomen (2011). Covariance measurement in the presence of non-synchronous trading and market microstructure noise. *Journal of Econometrics* 160(1), 58–68.
- Hayashi, T. and N. Yoshida (2005). On covariance estimation of non-synchronously observed diffusion processes. *Bernoulli* 11(2), 359–379.
- Huang, X. and G. Tauchen (2005). The relative contribution of jumps to total price variance. *Journal of Financial Econometrics* 3(4), 456–499.
- Jacod, J. and V. Todorov (2009). Testing for common arrivals of jumps for discretely observed multidimensional processes. *The Annals of Statistics* 37(4), 1792–1838.
- Jawadi, F., W. Louhichi, and A. I. Cheffou (2015). Testing and modeling jump contagion across international stock markets: A nonparametric intraday approach. *Journal of Financial Markets* 26, 64–84.
- Jiang, G. J. and C. Oomen, R (2008). Testing for jumps when asset prices are observed with noise - a swap variance approach. *Journal of Econometrics* 144(2), 352–370.
- Lahaye, J., S. Laurent, and C. J. Neely (2011). Jumps, cojumps and macro announcements. *Journal of Applied Econometrics* 26(6), 893–921.
- Lee, S. and P. A. Mykland (2008). Jumps in financial markets: a new nonparametric test and jump dynamics. *The Review of Financial Studies* 21, 2525–2563.
- Lee, S. S. and J. Hannig (2010). Detecting jumps from levy jump diffusion processes. *Journal of Financial Economics* 96(2), 271–290.
- Mallat, S. (1998). *A wavelet tour of signal processing*. Academic Press.
- Mancini, C. (2009). Non-parametric threshold estimation for models with stochastic diffusion coefficient and jumps. *Scandinavian Journal of Statistics* 36(2), 270–296.
- Mancini, C. and F. Gobbi (2012). Identifying the brownian covariation from the co-jumps given discrete observations. *Econometric Theory* 28(02), 249–273.

- Novotný, J., D. Petrov, and G. Urga (2015). Trading price jump clusters in foreign exchange markets. *Journal of Financial Markets* 24, 66–92.
- Percival, D. B. and H. Mofjeld (1997). Analysis of subtidal coastal sea level fluctuations using wavelets. *Journal of the American Statistical Association* 92(439), 886–880.
- Percival, D. B. and A. T. Walden (2000). *Wavelet Methods for Time series Analysis*. Cambridge University Press.
- Protter, P. (1992). *Stochastic integration and differential equations: A new approach*. New York: Springer-Verlag.
- Serroukh, A. and A. Walden (2000a). Wavelet scale analysis of bivariate time series i: motivation and estimation. *Journal of Nonparametric Statistics* 13(1), 1–36.
- Serroukh, A. and A. Walden (2000b). Wavelet scale analysis of bivariate time series ii: statistical properties for linear processes. *Journal of Nonparametric Statistics* 13(1), 37–56.
- Varneskov, R. T. (2016). Flat-top realized kernel estimation of quadratic covariation with non-synchronous and noisy asset prices. *Journal of Business & Economic Statistics* 34(1), 1–22.
- Voev, V. and A. Lunde (2007). Integrated covariance estimation using high-frequency data in the presence of noise. *Journal of Financial Econometrics* 5(1), 68–104.
- Wang, Y. (1995). Jump and sharp cusp detection via wavelets. *Biometrika* 82(2), 385–397.
- Whitcher, B., P. Guttorp, and D. B. Percival (1999). Mathematical background for wavelets estimators for cross covariance and cross correlation. 38, National Resource Centre for Supplementary Education.
- Whitcher, B., P. Guttorp, and D. B. Percival (2000). Wavelet analysis of covariance with application to atmospheric time series. *Journal of Geophysical Research* 105(D11), 941–962.
- Xue, Y., R. Gençay, and S. Fagan (2014). Jump detection with wavelets for high-frequency financial time series. *Quantitative Finance* 14(8), 1427–1444.
- Zhang, L. (2011). Estimating covariation: Epps effect, microstructure noise. *Journal of Econometrics* 160(1), 33–47.

Zhang, L., P. Mykland, and Y. Aït-Sahalia (2005). A tale of two time scales: Determining integrated volatility with noisy high frequency data. *Journal of the American Statistical Association* 100(472), 1394–1411.

## Appendix A. Discrete wavelet transform

Here, we briefly introduce a special form of the discrete wavelet transform called the maximal overlap discrete wavelet transform (MODWT). We demonstrate the application of the discrete-type wavelet transform using the pyramid algorithm (Mallat, 1998). This method is based on filtering time series (or stochastic process) with MODWT wavelet filters and then filtering the output again to obtain other wavelet scales. Using the MODWT procedure, we obtain wavelet and scaling coefficients that decompose analyzed stochastic processes into frequency bands (for more details and applications, see Percival and Mofjeld (1997), Percival and Walden (2000), and Gençay et al. (2002)).

The pyramid algorithm has several stages, and the number of stages depends on the maximal level of decomposition  $\mathcal{J}^m$ . Let us begin with the first stage. The wavelet coefficients at the first scale ( $j = 1$ ) are obtained via the circular filtering of time series  $X_{t,\ell}$  using the MODWT wavelet and scaling filters  $h_{1,l}$  and  $g_{1,l}$  (Percival and Walden, 2000) :

$$\mathcal{W}_{1,t}^\ell \equiv \sum_{l=0}^{L-1} h_{1,l} X_{(t-l \bmod N),\ell} \quad \mathcal{V}_{1,t}^\ell \equiv \sum_{l=0}^{L-1} g_{1,l} X_{(t-l \bmod N),\ell}. \quad (\text{A.1})$$

In the second step, the algorithm uses the scaling coefficients  $\mathcal{V}_{1,t}^\ell$  instead of  $X_{t,\ell}$ . The wavelet and scaling filters have a width  $L_j = 2^{j-1}(L-1) + 1$ . After filtering, we obtain the wavelet coefficients at scale  $j = 2$ :

$$\mathcal{W}_{2,t}^\ell \equiv \sum_{l=0}^{L-1} h_{2,l} \mathcal{V}_{(1,t-l \bmod N)}^\ell \quad \mathcal{V}_{2,t}^\ell \equiv \sum_{l=0}^{L-1} g_{2,l} \mathcal{V}_{(1,t-l \bmod N)}^\ell. \quad (\text{A.2})$$

The two steps of the algorithm create two vectors of the MODWT wavelet coefficients at scales  $j = 1$  and  $j = 2$ ;  $\mathcal{W}_{1,t}^\ell, \mathcal{W}_{2,t}^\ell$  and a vector of the MODWT wavelet scaling coefficients at scale two  $\mathcal{V}_{2,t}^\ell$  that is subsequently used for further decomposition. The vector  $\mathcal{W}_{1,t}^\ell$  represents the wavelet coefficients that reflect the activity at the frequency bands  $f[1/4, 1/2]$ ,  $\mathcal{W}_{2,t}^\ell$ :  $f[1/8, 1/4]$  and  $\mathcal{V}_{2,t}^\ell$ :  $f[0, 1/8]$ .

The transfer function of the wavelet filter  $h_l$  :  $l = 0, 1, \dots, L-1$ , where  $L$  is the width of the filter, is denoted as  $H(\cdot)$ . The pyramid algorithm exploits the fact that

if we increase the width of the filter to  $2^{j-1}(L-1)+1$ , the filter with the impulse response sequence has the form:

$$\{h_0, \underbrace{0, \dots, 0}_{2^{j-1}-1 \text{ zeros}}, h_1, \underbrace{0, \dots, 0}_{2^{j-1}-1 \text{ zeros}}, h_{L-2}, \underbrace{0, \dots, 0}_{2^{j-1}-1 \text{ zeros}}, h_L\}, \quad (\text{A.3})$$

and a transfer function defined as  $H(2^{j-1}f)$ . Then, the pyramid algorithm takes on the following form:

$$\mathcal{W}_{j,t}^\ell \equiv \sum_{l=0}^{L-1} h_l \mathcal{V}_{(j-1,t-2^{j-1}l \bmod N)}^\ell \quad t=0, 1, \dots, N-1, \quad (\text{A.4})$$

$$\mathcal{V}_{j,t}^\ell \equiv \sum_{l=0}^{L-1} g_l \mathcal{V}_{(j-1,t-2^{j-1}l \bmod N)}^\ell \quad t=0, 1, \dots, N-1, \quad (\text{A.5})$$

where in the first stage, we set  $X = \mathcal{V}_{0,t}^\ell$ . After applying the MODWT, we obtain  $j \leq \mathcal{J}^m \leq \log_2(N)$  vectors of wavelet coefficients and one vector of scaling coefficients. The  $j$ -th level wavelet coefficients in vector  $\mathcal{W}_{j,t}^\ell$  represent the frequency bands  $f[1/2^{j+1}, 1/2^j]$ , whereas the  $j$ -th level scaling coefficients in vector  $\mathcal{V}_{j,t}^\ell$  represent  $f[0, 1/2^{j+1}]$ . In our analysis, we use the MODWT with the Daubechies wavelet filter D(4) and reflecting boundary conditions.

## Appendix B. Wavelet covariance

Let  $(X_{t,\ell_1}, X_{t,\ell_2})$  be a covariance stationary process with the square integrable spectral density functions  $S^{\ell_1}(\cdot)$ ,  $S^{\ell_2}(\cdot)$  and cross spectra  $S^{\ell_1, \ell_2}(\cdot)$ . Using the Daubechies family wavelet with length  $L=4$ , we can use generally non-stationary processes that are stationary after the  $d$ -th difference, where  $d \leq L/2$ . The wavelet covariance of  $(X_{t,\ell_1}, X_{t,\ell_2})$  at level  $j$  is defined as:

$$\gamma_j^{\ell_1, \ell_2} = \text{Cov}(\mathcal{W}_{j,t}^{\ell_1}, \mathcal{W}_{j,t}^{\ell_2}). \quad (\text{B.1})$$

For a particular level of decomposition  $\mathcal{J}^m \leq \log_2(T)$ , the covariance of  $(X_{t,\ell_1}, X_{t,\ell_2})$  is a sum of the covariances of the MODWT wavelet coefficients  $\gamma_j^{\ell_1, \ell_2}$  at all scales  $j=1, 2, \dots, \mathcal{J}^m$  and the covariance of the scaling coefficients  $\mathcal{V}_{\mathcal{J}^m,t}^\ell$  at scale  $\mathcal{J}^m$ :

$$\text{Cov}(X_{t,\ell_1}, X_{t,\ell_2}) = \text{Cov}(\mathcal{V}_{\mathcal{J}^m,t}^{\ell_1}, \mathcal{V}_{\mathcal{J}^m,t}^{\ell_2}) + \sum_{j=1}^{\mathcal{J}^m} \gamma_j^{\ell_1, \ell_2}. \quad (\text{B.2})$$

For process  $(X_{t,\ell_1}, X_{t,\ell_2})$  defined above, the estimator of a wavelet covariance at level  $j$  is defined as

$$\hat{\gamma}_j^{\ell_1, \ell_2} = \frac{1}{M_j} \sum_{t=L_j-1}^{N-1} \mathcal{W}_{j,t}^{\ell_1} \mathcal{W}_{j,t}^{\ell_2}, \quad (\text{B.3})$$

where  $M_j = N - L_j + 1 > 0$  is number of the  $j$ -th level MODWT coefficients for both processes that are unaffected by the boundary conditions. Whitcher et al. (1999) prove that for the Gaussian process  $(X_{t,\ell_1}, X_{t,\ell_2})$ , the MODWT estimator of wavelet covariance is unbiased and asymptotically normally distributed.

**Proposition 1.** *When  $\mathcal{J}^m \rightarrow \infty$ , the covariance of the scaling coefficients  $(\mathcal{V}_{\mathcal{J}^m,t}^{\ell_1}, \mathcal{V}_{\mathcal{J}^m,t}^{\ell_2})$  goes to zero (Whitcher et al., 1999), and thus, we can rewrite (B.2) as:*

$$\text{Cov}(X_{t,\ell_1}, X_{t,\ell_2}) = \sum_{j=1}^{\infty} \gamma_j^{\ell_1, \ell_2}. \quad (\text{B.4})$$

**Proof:** To prove Proposition 1, we write the covariance of the MODWT wavelet coefficients in the form:

$$\gamma_j^{\ell_1, \ell_2} = \int_{-1/2}^{1/2} \mathcal{H}_j(f) S^{\ell_1, \ell_2}(f) df, \quad (\text{B.5})$$

where  $\mathcal{H}_j(f)$  denotes the squared gain function of the wavelet MODWT filter  $h_j$ . The covariance of the scaling coefficients at level  $\mathcal{J}^m$  (the last level of decomposition):

$$\text{Cov}(\mathcal{V}_{\mathcal{J}^m,t}^{\ell_1}, \mathcal{V}_{\mathcal{J}^m,t}^{\ell_2}) = \int_{-1/2}^{1/2} \mathcal{G}_J(f) S^{\ell_1, \ell_2}(f) df, \quad (\text{B.6})$$

where  $\mathcal{G}_{\mathcal{J}^m}(f)$  denotes the squared gain function of the scaling MODWT filter  $g_{\mathcal{J}^m}$ , such that  $\mathcal{G}_{\mathcal{J}^m}(f) \equiv \prod_{l=0}^{\mathcal{J}^m-1} \mathcal{G}(2^l f)$ . When  $\mathcal{H}(f) + \mathcal{G}(f) = 1$  (Percival and Walden, 2000), the covariance decomposed by wavelets at the first level ( $\mathcal{J}^m = 1$ ) only is obtained as the sum of the wavelet and scaling MODWT coefficients' covariances,

$$\text{Cov}(X_{t,\ell_1}, X_{t,\ell_2}) = \int_{-1/2}^{1/2} (\mathcal{H}(f) + \mathcal{G}(f)) S^{\ell_1, \ell_2}(f) df = \text{Cov}(\mathcal{V}_{1,t}^{\ell_1}, \mathcal{V}_{1,t}^{\ell_2}) + \gamma_1^{\ell_1, \ell_2}. \quad (\text{B.7})$$

Further, we assume that this also holds for level  $\mathcal{J}^m - 1$ :

$$\text{Cov}(X_{t,\ell_1}, X_{t,\ell_2}) = \text{Cov}(\mathcal{V}_{\mathcal{J}^m-1,t}^{\ell_1}, \mathcal{V}_{\mathcal{J}^m-1,t}^{\ell_2}) + \sum_{j=1}^{\mathcal{J}^m-1} \gamma_j^{\ell_1, \ell_2}. \quad (\text{B.8})$$

Following Whitcher et al. (1999), we have

$$\begin{aligned}
Cov(\mathcal{V}_{\mathcal{J}^m-1,t}^{\ell_1}, \mathcal{V}_{\mathcal{J}^m-1,t}^{\ell_2}) &= \int_{-1/2}^{1/2} \mathcal{G}_{\mathcal{J}^m-1}(f) S^{\ell_1, \ell_2}(f) df \\
&= \int_{-1/2}^{1/2} \left[ \prod_{l=0}^{\mathcal{J}^m-2} \mathcal{G}(2^l f) \right] S^{\ell_1, \ell_2}(f) df \\
&= \int_{-1/2}^{1/2} [\mathcal{G}(2^{\mathcal{J}^m-1} f) + \mathcal{H}(2^{\mathcal{J}^m-1} f)] \left[ \prod_{l=0}^{\mathcal{J}^m-2} \mathcal{G}(2^l f) \right] S^{\ell_1, \ell_2}(f) df \\
&= \int_{-1/2}^{1/2} [\mathcal{G}_{\mathcal{J}^m}(f) + \mathcal{H}_{\mathcal{J}^m}(f)] S^{\ell_1, \ell_2}(f) df \\
&= Cov(\mathcal{V}_{\mathcal{J}^m,t}^{\ell_1}, \mathcal{V}_{\mathcal{J}^m,t}^{\ell_2}) + \gamma_j^{\ell_1, \ell_2}, \tag{B.9}
\end{aligned}$$

which proves, by induction, the wavelet covariance decomposition of  $(X_{t,\ell_1}, X_{t,\ell_2})$  for a finite number of scales  $\mathcal{J}^m$ .

We also prove that as  $\mathcal{J}^m \rightarrow \infty$ , the covariance between the scaling coefficients goes to zero; therefore, the covariance of  $(X_{t,\ell_1}, X_{t,\ell_2})$  depends only on the covariance of the wavelet coefficients  $\gamma_j^{\ell_1, \ell_2}$ . Using the result (B.9), we can write:

$$Cov(\mathcal{V}_{\mathcal{J}^m-1,t}^{\ell_1}, \mathcal{V}_{\mathcal{J}^m-1,t}^{\ell_2}) = Cov(\mathcal{V}_{\mathcal{J}^m,t}^{\ell_1}, \mathcal{V}_{\mathcal{J}^m,t}^{\ell_2}) + \gamma_j^{\ell_1, \ell_2} \tag{B.10}$$

$$Cov(\mathcal{V}_{\mathcal{J}^m,t}^{\ell_1}, \mathcal{V}_{\mathcal{J}^m,t}^{\ell_2}) = Cov(\mathcal{V}_{\mathcal{J}^m+1,t}^{\ell_1}, \mathcal{V}_{\mathcal{J}^m+1,t}^{\ell_2}) + \gamma_{\mathcal{J}^m+1}^{\ell_1, \ell_2} \tag{B.11}$$

$$\vdots = \vdots \tag{B.12}$$

$$Cov(\mathcal{V}_{\mathcal{J}^m+n-1,t}^{\ell_1}, \mathcal{V}_{\mathcal{J}^m+n-1,t}^{\ell_2}) = Cov(\mathcal{V}_{\mathcal{J}^m+n,t}^{\ell_1}, \mathcal{V}_{\mathcal{J}^m+n,t}^{\ell_2}) + \gamma_{\mathcal{J}^m+n}^{\ell_1, \ell_2}. \tag{B.13}$$

By summation, we obtain

$$Cov(\mathcal{V}_{\mathcal{J}^m-1,t}^{\ell_1}, \mathcal{V}_{\mathcal{J}^m-1,t}^{\ell_2}) = Cov(\mathcal{V}_{\mathcal{J}^m+n,t}^{\ell_1}, \mathcal{V}_{\mathcal{J}^m+n,t}^{\ell_2}) + \sum_{j=0}^n \gamma_{\mathcal{J}^m+j}^{\ell_1, \ell_2}. \tag{B.14}$$

For the part consisting of the wavelet coefficient covariance, we have

$$\sum_{j=0}^n \gamma_{\mathcal{J}^m+j}^{\ell_1, \ell_2} = Cov(\mathcal{V}_{\mathcal{J}^m-1,t}^{\ell_1}, \mathcal{V}_{\mathcal{J}^m-1,t}^{\ell_2}) - Cov(\mathcal{V}_{\mathcal{J}^m+n,t}^{\ell_1}, \mathcal{V}_{\mathcal{J}^m+n,t}^{\ell_2}). \tag{B.15}$$

Let us denote  $s_r$  as a sum of the wavelet coefficients covariances up to scale  $r$ , i.e.,

$$s_r = \sum_{j=0}^r \gamma_j^{\ell_1, \ell_2}. \tag{B.16}$$

Then, for any positive integer  $r$  such that  $r > \mathcal{J}^m$ , we have:

$$s_r = \sum_{j=0}^{\mathcal{J}^m-1} \gamma_j^{\ell_1, \ell_2} + \sum_{j=0}^{r-\mathcal{J}^m} \gamma_{\mathcal{J}^m+j}^{\ell_1, \ell_2} \quad (\text{B.17})$$

$$= \text{Cov}(\mathcal{V}_{\mathcal{J}^m-1,t}^{\ell_1}, \mathcal{V}_{\mathcal{J}^m-1,t}^{\ell_2}) - \text{Cov}(\mathcal{V}_{r,t}^{\ell_1}, \mathcal{V}_{r,t}^{\ell_2}) + \sum_{j=0}^{\mathcal{J}^m-1} \gamma_j^{\ell_1, \ell_2}. \quad (\text{B.18})$$

Hence, for any two positive integers  $r_1, r_2 > \mathcal{J}^m$ , we can write

$$|s_{r_1} - s_{r_2}| = |\text{Cov}(\mathcal{V}_{r_1,t}^{\ell_1}, \mathcal{V}_{r_1,t}^{\ell_2}) - \text{Cov}(\mathcal{V}_{r_2,t}^{\ell_1}, \mathcal{V}_{r_2,t}^{\ell_2})|. \quad (\text{B.19})$$

Based on the result of Whitcher et al. (2000) (lemma 1, page 2), for any  $\epsilon > 0$ , there exists  $\mathcal{J}_\epsilon^m$  such that for a positive integer,  $r > \mathcal{J}_\epsilon^m$  holds:

$$|\text{Cov}(\mathcal{V}_{r,t}^{\ell_1}, \mathcal{V}_{r,t}^{\ell_2})| < \epsilon. \quad (\text{B.20})$$

Then (B.20), for any  $\epsilon > 0$ , there exists  $\mathcal{J}_\epsilon^m$  such that for positive integers  $r_1, r_2 > \mathcal{J}_\epsilon^m$ , we obtain

$$|s_{r_1} - s_{r_2}| \leq 2\epsilon, \quad (\text{B.21})$$

As a result, the sequence  $\{s_r\}$  is Cauchy and has a limit:

$$\lim_{r \rightarrow \infty} s_r = \sum_{j=0}^{\infty} \gamma_j^{\ell_1, \ell_2} = \text{Cov}(\mathcal{V}_{\mathcal{J}^m-1,t}^{\ell_1}, \mathcal{V}_{\mathcal{J}^m-1,t}^{\ell_2}) + \sum_{j=0}^{\mathcal{J}^m-1} \gamma_j^{\ell_1, \ell_2}. \quad (\text{B.22})$$

Then, it follows that

$$\sum_{j=\mathcal{J}^m}^{\infty} \gamma_j^{\ell_1, \ell_2} = \text{Cov}(\mathcal{V}_{\mathcal{J}^m-1,t}^{\ell_1}, \mathcal{V}_{\mathcal{J}^m-1,t}^{\ell_2}), \quad (\text{B.23})$$

which implies (c.f. B.8)

$$\text{Cov}(X_{t,\ell_1}, X_{t,\ell_2}) = \sum_{j=0}^{\infty} \gamma_j^{\ell_1, \ell_2}, \quad (\text{B.24})$$

This completes the proof. □

## Appendix C. Tables and Figures

Table C.1:  $\Sigma_t^{12}$  Bias (variance in parenthesis)  $\times 10^4$  of all estimators from 10,000 simulations of the jump-diffusion model with  $\epsilon_1 = 0$ ,  $\epsilon_2 = 0.0015$ , zero and one co-jump (CJ), and zero and one independent jump (IJ). RC – realized covariance estimator, BC – bipower covariance estimator, TSCV – two-scale realized covariance, MRK – multivariate realized kernel, JWTSCV – jump wavelet two-scale realized covariance with sampling at 1-min, 5-min, 30-min and 1-hour intervals.

		RC	BC	TSCV	MRK	JWTSCV	
Zero Noise ( $\epsilon_1$ )							
Zero IJ	Zero CJ	1-min	-0.001 (0.015)	-0.002 (0.017)	-0.005 (0.013)	-0.006 (0.042)	-0.005 (0.013)
		5-min	0.001 (0.035)	-0.002 (0.040)	-0.002 (0.029)	-0.008 (0.069)	-0.002 (0.029)
		30-min	-0.001 (0.085)	-0.015 (0.090)	-0.015 (0.067)	-0.040 (0.112)	-0.015 (0.067)
		1-hour	0.002 (0.124)	-0.032 (0.124)	-0.030 (0.091)	-0.080 (0.129)	-0.030 (0.091)
	One CJ	1-min	0.990 (1.786)	0.047 (0.089)	0.969 (1.755)	0.982 (1.805)	-0.004 (0.012)
		5-min	0.988 (1.811)	0.107 (0.245)	0.962 (1.772)	0.960 (1.834)	-0.005 (0.029)
		30-min	1.019 (2.041)	0.241 (0.577)	0.895 (1.705)	0.743 (1.617)	-0.018 (0.065)
		1-hour	1.001 (1.925)	0.272 (0.745)	0.753 (1.564)	0.444 (1.335)	-0.036 (0.090)
One IJ	Zero CJ	1-min	-0.003 (0.042)	0.035 (0.042)	-0.006 (0.036)	-0.000 (0.155)	-0.004 (0.012)
		5-min	-0.006 (0.115)	0.063 (0.093)	-0.008 (0.090)	-0.014 (0.218)	-0.005 (0.028)
		30-min	0.012 (0.326)	0.097 (0.209)	-0.007 (0.266)	-0.021 (0.467)	-0.014 (0.066)
		1-hour	-0.008 (0.568)	0.069 (0.341)	-0.038 (0.384)	-0.096 (0.547)	-0.035 (0.090)
	One CJ	1-min	0.926 (1.624)	0.084 (0.107)	0.907 (1.593)	0.917 (1.632)	-0.005 (0.012)
		5-min	1.002 (1.795)	0.197 (0.343)	0.988 (1.781)	0.968 (1.860)	-0.005 (0.028)
		30-min	1.012 (1.892)	0.417 (0.758)	0.910 (1.768)	0.771 (1.800)	-0.018 (0.069)
		1-hour	1.013 (2.097)	0.493 (1.113)	0.797 (1.730)	0.469 (1.586)	-0.038 (0.091)
Noise ( $\epsilon_2$ )							
Zero IJ	Zero CJ	1-min	0.000 (0.015)	-0.000 (0.017)	-0.004 (0.013)	-0.002 (0.045)	-0.004 (0.013)
		5-min	-0.002 (0.035)	-0.004 (0.040)	-0.005 (0.028)	-0.009 (0.069)	-0.005 (0.028)
		30-min	0.004 (0.091)	-0.016 (0.095)	-0.015 (0.071)	-0.036 (0.130)	-0.015 (0.071)
		1-hour	-0.000 (0.124)	-0.036 (0.125)	-0.036 (0.087)	-0.086 (0.123)	-0.036 (0.087)
	One CJ	1-min	1.016 (1.745)	0.047 (0.068)	0.993 (1.710)	0.999 (1.739)	-0.005 (0.013)
		5-min	0.882 (1.597)	0.099 (0.252)	0.866 (1.605)	0.874 (1.691)	-0.004 (0.028)
		30-min	1.024 (1.850)	0.261 (0.632)	0.948 (1.774)	0.831 (1.838)	-0.018 (0.062)
		1-hour	0.982 (1.834)	0.292 (0.719)	0.789 (1.615)	0.490 (1.371)	-0.035 (0.093)
One IJ	Zero CJ	1-min	0.001 (0.049)	0.037 (0.045)	-0.003 (0.039)	-0.001 (0.196)	-0.004 (0.012)
		5-min	0.007 (0.094)	0.068 (0.099)	-0.001 (0.084)	-0.014 (0.248)	-0.005 (0.029)
		30-min	0.015 (0.362)	0.097 (0.211)	0.002 (0.268)	-0.030 (0.523)	-0.018 (0.066)
		1-hour	0.017 (0.536)	0.072 (0.307)	-0.028 (0.370)	-0.074 (0.449)	-0.033 (0.092)
	One CJ	1-min	0.832 (1.443)	0.076 (0.084)	0.815 (1.418)	0.831 (1.472)	-0.005 (0.012)
		5-min	1.042 (1.818)	0.228 (0.473)	1.031 (1.806)	1.015 (1.995)	-0.004 (0.029)
		30-min	0.977 (1.865)	0.448 (0.782)	0.886 (1.678)	0.763 (1.704)	-0.018 (0.067)
		1-hour	0.993 (1.957)	0.501 (1.080)	0.812 (1.698)	0.515 (1.617)	-0.037 (0.088)



Table C.2: Correlation bias (variance in parenthesis) of all estimators from 10,000 simulations of the jump-diffusion model with  $\epsilon_1 = 0$ ,  $\epsilon_2 = 0.0015$ , zero and one co-jump (CJ), and zero and one independent jump (IJ). RC – realized covariance estimator, BC – bipower covariance estimator, TSCV – two-scale realized covariance, MRK – multivariate realized kernel, JWTSCV – jump wavelet two-scale realized covariance with sampling at 1-min, 5-min, 30-min and 1-hour intervals.

		RC	BC	TSCV	MRK	JWTSCV	
Zero Noise ( $\epsilon_1$ )							
Zero IJ	Zero CJ	1-min	-0.001 (0.009)	-0.001 (0.013)	-0.001 (0.007)	-0.003 (0.027)	-0.001 (0.007)
		5-min	-0.001 (0.020)	-0.001 (0.029)	-0.000 (0.016)	-0.005 (0.045)	-0.000 (0.016)
		30-min	-0.007 (0.056)	-0.004 (0.091)	-0.003 (0.042)	-0.019 (0.111)	-0.003 (0.042)
		1-hour	-0.013 (0.095)	-0.011 (0.164)	-0.005 (0.069)	-0.030 (0.207)	-0.005 (0.069)
	One CJ	1-min	0.037 (0.036)	0.010 (0.020)	0.037 (0.036)	0.036 (0.041)	0.000 (0.007)
		5-min	0.037 (0.039)	0.014 (0.037)	0.037 (0.038)	0.035 (0.051)	-0.001 (0.017)
		30-min	0.037 (0.052)	0.029 (0.076)	0.037 (0.048)	0.031 (0.081)	-0.005 (0.044)
		1-hour	0.027 (0.087)	0.017 (0.157)	0.029 (0.072)	-0.007 (0.213)	-0.013 (0.078)
One IJ	Zero CJ	1-min	-0.492 (0.283)	-0.021 (0.055)	-0.492 (0.282)	-0.494 (0.301)	-0.001 (0.007)
		5-min	-0.464 (0.306)	-0.035 (0.092)	-0.460 (0.300)	-0.466 (0.342)	-0.001 (0.016)
		30-min	-0.483 (0.364)	-0.102 (0.276)	-0.473 (0.342)	-0.488 (0.461)	-0.002 (0.043)
		1-hour	-0.504 (0.456)	-0.194 (0.450)	-0.476 (0.398)	-0.512 (0.620)	-0.012 (0.078)
	One CJ	1-min	-0.331 (0.301)	-0.007 (0.055)	-0.330 (0.300)	-0.333 (0.312)	-0.001 (0.007)
		5-min	-0.343 (0.313)	-0.021 (0.136)	-0.342 (0.312)	-0.355 (0.351)	-0.002 (0.016)
		30-min	-0.340 (0.355)	-0.060 (0.258)	-0.332 (0.337)	-0.346 (0.435)	-0.007 (0.047)
		1-hour	-0.368 (0.434)	-0.111 (0.430)	-0.347 (0.391)	-0.398 (0.593)	-0.012 (0.076)
Noise ( $\epsilon_2$ )							
Zero IJ	Zero CJ	1-min	-0.000 (0.009)	-0.000 (0.013)	0.000 (0.007)	-0.002 (0.028)	0.000 (0.007)
		5-min	-0.002 (0.020)	-0.001 (0.030)	-0.001 (0.016)	-0.005 (0.046)	-0.001 (0.016)
		30-min	-0.002 (0.052)	-0.005 (0.086)	-0.002 (0.043)	-0.014 (0.107)	-0.002 (0.043)
		1-hour	-0.011 (0.093)	-0.011 (0.171)	-0.006 (0.067)	-0.048 (0.249)	-0.006 (0.067)
	One CJ	1-min	0.039 (0.037)	0.010 (0.019)	0.039 (0.037)	0.038 (0.041)	-0.000 (0.007)
		5-min	0.037 (0.039)	0.015 (0.034)	0.037 (0.037)	0.035 (0.049)	-0.001 (0.017)
		30-min	0.036 (0.054)	0.021 (0.082)	0.036 (0.049)	0.027 (0.091)	-0.005 (0.043)
		1-hour	0.028 (0.092)	0.018 (0.153)	0.033 (0.066)	0.010 (0.187)	-0.012 (0.078)
One IJ	Zero CJ	1-min	-0.477 (0.287)	-0.018 (0.058)	-0.477 (0.286)	-0.479 (0.310)	-0.000 (0.007)
		5-min	-0.470 (0.302)	-0.042 (0.106)	-0.469 (0.298)	-0.481 (0.343)	-0.002 (0.016)
		30-min	-0.489 (0.355)	-0.112 (0.264)	-0.476 (0.328)	-0.485 (0.445)	-0.006 (0.045)
		1-hour	-0.482 (0.428)	-0.154 (0.463)	-0.467 (0.392)	-0.483 (0.594)	-0.012 (0.079)
	One CJ	1-min	-0.344 (0.293)	-0.011 (0.047)	-0.344 (0.293)	-0.346 (0.306)	-0.001 (0.007)
		5-min	-0.347 (0.311)	-0.014 (0.141)	-0.345 (0.305)	-0.358 (0.349)	-0.002 (0.016)
		30-min	-0.345 (0.359)	-0.051 (0.269)	-0.337 (0.345)	-0.347 (0.441)	-0.006 (0.044)
		1-hour	-0.360 (0.417)	-0.133 (0.415)	-0.345 (0.381)	-0.368 (0.567)	-0.012 (0.077)

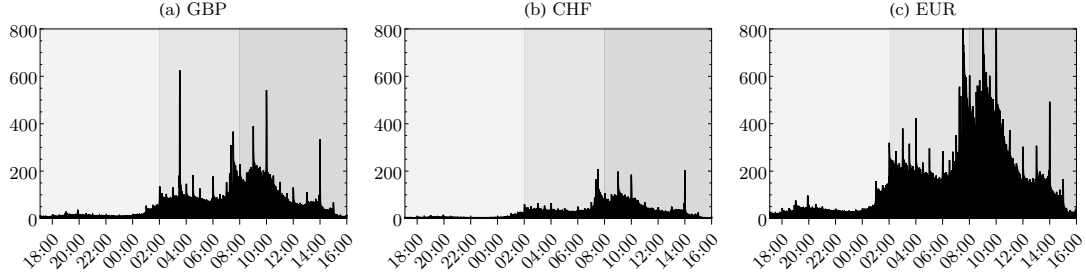


Figure C.1: Trading activity on (a) GBP, (b) CHF, and (c) EUR future contracts measured in terms of the average volume using 1-minute trading intervals over the whole period of January 5, 2007 – July 3, 2015. The trading session hours from Asia (17:00 – 2:00 CST) to Europe (2:00 – 8:00 CST) and then to the U.S. (8:00 – 16:00 CST) are highlighted by different background shades.

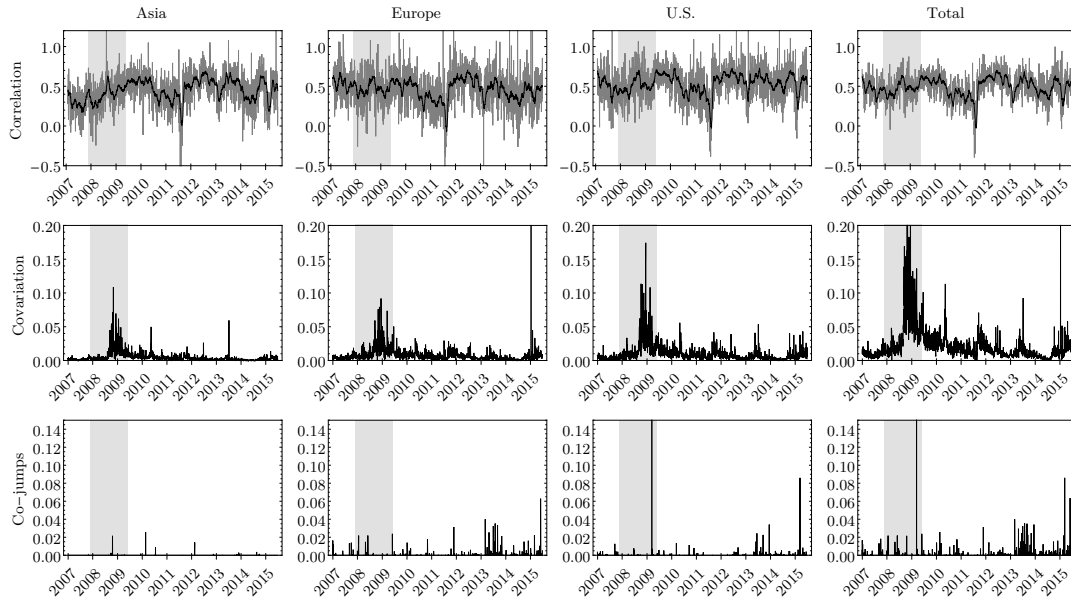


Figure C.2: **GBP-CHF pair**: Realized correlation in gray with a 21-day moving average in black (upper row), integrated covariance (middle row), and co-jumps (lower row) estimated by JWTSCV. The quantities computed during the Asian, European, and U.S. sessions are depicted in the first three columns. The last column lists the quantities computed over a whole trading day session. A 2007 – 2008 crisis period is shaded.

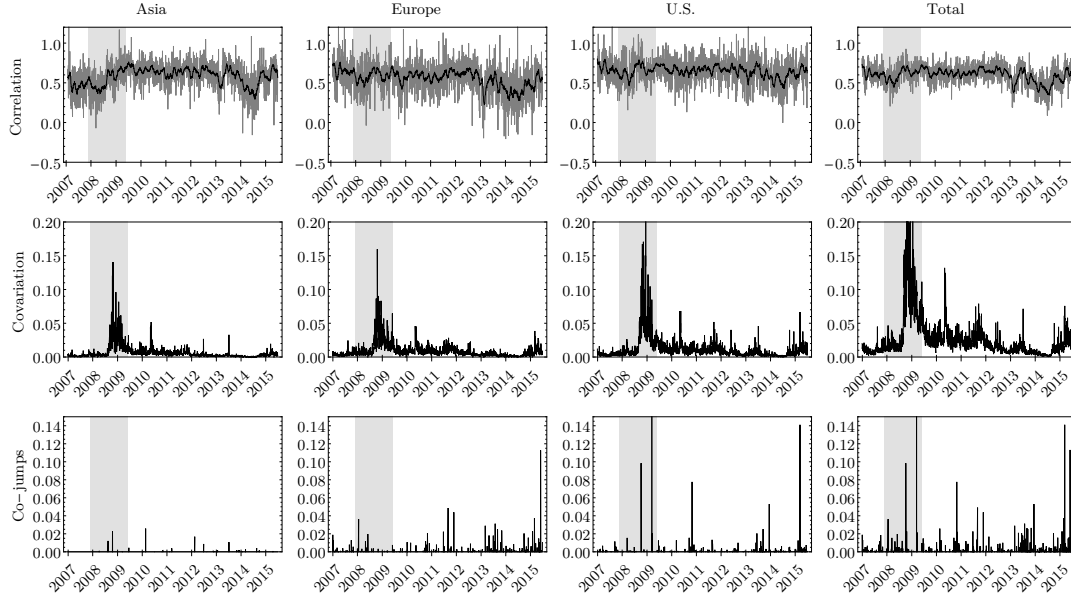


Figure C.3: **GBP–EUR pair**: Realized correlation in gray with a 21-day moving average in black (upper row), integrated covariance (middle row), and co-jumps (lower row) estimated using JWTSCV. The quantities computed during the Asian, European, and U.S. sessions are depicted in the first three columns. The last column lists the quantities computed over a whole trading day session. The 2007 – 2008 crisis period is shaded.

Table C.3: Correlations measured during the Asia, EU, and U.S. trading hours.

	Asia	EU	U.S.	Total
GBP–CHF	0.446	0.465	0.536	0.489
GBP–EUR	0.583	0.558	0.649	0.599
CHF–EUR	0.650	0.764	0.753	0.740

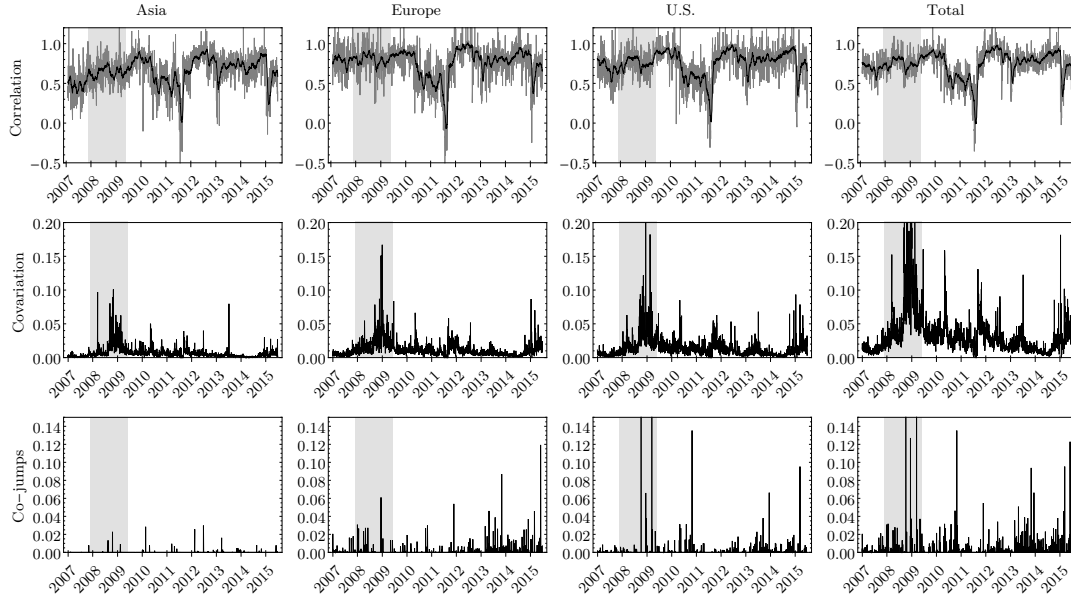


Figure C.4: **CHF–EUR pair**: Realized correlation in gray with a 21-day moving average in black (upper row), integrated covariance (middle row), and co-jumps (middle row) estimated using JWTSCV. The quantities computed during the Asian, European, and U.S. sessions are depicted in the first three columns. The last column lists the quantities computed over a whole trading day session. The 2007 – 2008 crisis period is shaded.

Table C.4: Number of days with negative co-jumps during the Asia, EU and the U.S. trading hours and the percentages of negative co-jumps among all co-jumps for a given market

	Asia		EU		U.S.		Total
	#	%	#	%	#	%	
GBP–CHF	4	15.4%	10	6.2%	2	1.3%	16
GBP–EUR	0	0%	17	8.3%	5	2.6%	22
CHF–EUR	4	6.7%	5	1.7%	2	0.7%	11

Table C.5: Number of days with co-jumps (CJ), co-jump covariation, covariance and the ratio of co-jumps to covariance (maximum values are shown in bold).

		Asia		EU		U.S.		Total
		#	%	#	%	#	%	
GBP–CHF	Days with CJ	26	7.7	162	<b>48.1</b>	149	44.2	337
	CJ cov	-	5.6	-	<b>52</b>	-	42.4	-
	Cov	0.046	21.8	0.073	34.6	0.092	<b>43.6</b>	0.211
	% CJ cov/cov	-	0.3	-	<b>2.8</b>	-	1.7	-
GBP–EUR	Days with CJ	35	8.2	204	<b>47.5</b>	190	44.3	429
	CJ cov	-	5.8	-	<b>47.6</b>	-	46.6	-
	Cov	0.061	23.6	0.087	33.7	0.110	<b>42.6</b>	0.257
	% CJ cov/cov	-	0.5	-	<b>3.6</b>	-	2.1	-
CHF–EUR	Days with CJ	60	9.1	297	44.9	304	<b>46.0</b>	661
	CJ cov	-	6.1	-	45.6	-	<b>48.3</b>	-
	Cov	0.066	20.9	0.114	36.1	0.136	<b>43.0</b>	0.315
	% CJ cov/cov	-	0.8	-	<b>4.2</b>	-	3.4	-

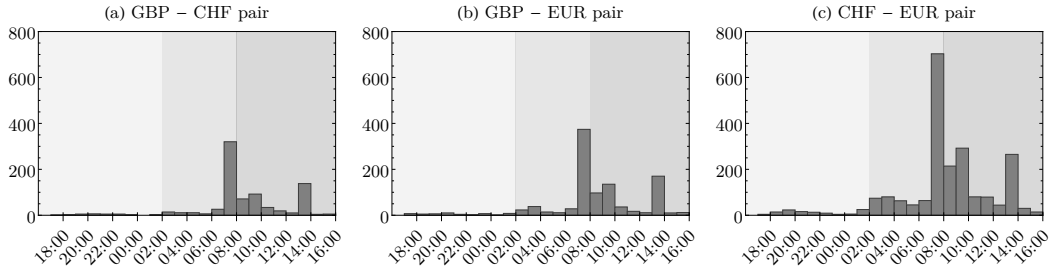


Figure C.5: Distribution of co-jumps during trading sessions starting with Asia (17:00 – 2:00 CST), then Europe (2:00 – 8:00 CST), and then the U.S. (8:00 – 16:00 CST) highlighted using different background shades.

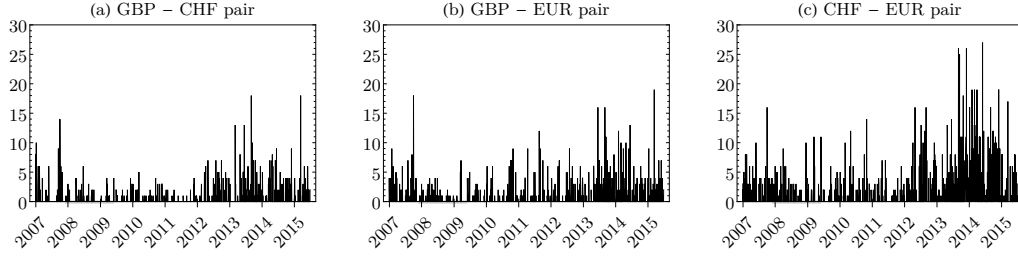


Figure C.6: Number of co-jumps for all three currency pairs during 2007 – 2015.

Table C.6: Dynamics of the ratio of co-jumps to covariance (maximum values are shown in bold)

		2007	2008	2009	2010	2011	2012	2013	2014	2015
GBP–CHF	Asia	0.06	0.19	0.07	0.61	0.07	0.47	<b>0.73</b>	0.52	0.01
	EU	2.60	1.80	0.75	1.10	0.74	2.50	<b>6.80</b>	5.30	4.30
	U.S.	3.00	0.73	1.00	0.88	0.25	1.70	<b>3.20</b>	2.90	1.90
	Total	2.90	2.10	1.10	1.40	0.70	2.20	<b>6.30</b>	6.20	4.00
GBP–EUR	Asia	0.01	0.45	0.17	0.50	0.10	0.94	<b>1.00</b>	0.93	0.16
	EU	3.30	2.00	2.80	1.60	2.70	1.90	6.50	<b>7.00</b>	5.30
	U.S.	2.80	1.00	1.20	2.10	1.20	1.60	<b>3.10</b>	2.90	3.30
	Total	3.20	2.00	1.40	2.40	2.00	2.20	<b>6.20</b>	6.10	5.60
CHF–EUR	Asia	0.10	0.43	0.12	0.58	0.61	0.87	<b>2.60</b>	1.30	0.37
	EU	3.70	2.00	0.96	2.00	1.20	4.20	8.40	<b>12.00</b>	4.70
	U.S.	3.00	1.40	1.80	3.80	1.90	3.20	6.00	<b>7.20</b>	1.90
	Total	3.60	2.20	1.70	3.60	2.20	4.10	8.70	<b>11.00</b>	4.10